












Enhanced RNA-targeting CRISPR-Cas technology in zebrafish

Received: 13 July 2024

Accepted: 28 February 2025

Published online: 16 March 2025



Ismael Moreno-Sánchez ^{1,2,3,10}, Luis Hernández-Huertas^{1,2,10}, Daniel Nahón-Cano^{1,2,10}, Pedro Manuel Martínez-García ¹, Anthony J. Treichel⁴, Carlos Gómez-Marin^{1,2}, Laura Tomás-Gallardo ^{1,5}, Gabriel da Silva Pescador⁴, Gopal Kushawah⁴, Rhonda Egidy⁴, Anoja Perera⁴, Alejandro Díaz-Moscoso ^{1,5,9}, Alejandra Cano-Ruiz ^{1,2}, John A. Walker II⁶, Manuel J. Muñoz ^{1,2}, Kevin Holden ⁶, Joan Galcerán ^{3,7}, M. Ángela Nieto ^{3,7}, Ariel A. Bazzini ^{4,8} & Miguel A. Moreno-Mateos ^{1,2} ✉

CRISPR-Cas13 RNA-targeting systems are widely used in basic and applied sciences. However, its application has recently generated controversy due to collateral activity in mammalian cells and mouse models. Moreover, its competence could be improved in vivo. Here, we optimized transient formulations as ribonucleoprotein complexes or mRNA-gRNA combinations to enhance the CRISPR-RfxCas13d system in zebrafish. We i) use chemically modified gRNAs to allow more penetrant loss-of-function phenotypes, ii) improve nuclear RNA targeting, and iii) compare different computational models and determine the most accurate to predict gRNA activity in vivo. Furthermore, we demonstrate that transient CRISPR-RfxCas13d can effectively deplete endogenous mRNAs in zebrafish embryos without inducing collateral effects, except when targeting extremely abundant and ectopic RNAs. Finally, we implement alternative RNA-targeting CRISPR-Cas systems such as CRISPR-Cas7-11 and CRISPR-DjCas13d. Altogether, these findings contribute to CRISPR-Cas technology optimization for RNA targeting in zebrafish through transient approaches and assist in the progression of in vivo applications.

RfxCas13d is a class 2/type VI CRISPR-Cas RNA endonuclease from *Ruminococcus flavefaciens* XPD3002 (also called CasRx) that together with a guide RNA (gRNA) targets RNA by RNA-RNA hybridization¹. The CRISPR-RfxCas13d system has been efficiently used to eliminate RNA and therefore possesses extraordinary potential for biotechnology and biomedicine^{2–9}. We recently optimized this technology in vivo using ribonucleoprotein (RNP)

complexes or mRNA-gRNA delivery^{10–14} allowing effective, transient, and cytosolic mRNA knockdown (KD) during vertebrate embryogenesis, including zebrafish, medaka, killifish, and mouse, among other vertebrate embryos^{10–21}. Beyond, these approaches have been recently used to label mRNAs during zebrafish embryogenesis expanding the applications of the technology in vivo²². However, through our continued work we have identified a set of limitations

¹Andalusian Center for Developmental Biology (CABD), Pablo de Olavide University/CSIC/Junta de Andalucía, Seville, Spain. ²Department of Molecular Biology and Biochemical Engineering, Pablo de Olavide University, Seville, Spain. ³Instituto de Neurociencias (CSIC-UMH), Alicante, Spain. ⁴Stowers Institute for Medical Research, Kansas City, MO, USA. ⁵Proteomics and Biochemistry Platform, Andalusian Center for Developmental Biology (CABD), Pablo de Olavide University/CSIC/Junta de Andalucía, Seville, Spain. ⁶Synthego Corporation, Redwood City, CA, USA. ⁷CIBERER, Centro de Investigación Biomédica en Red de Enfermedades Raras, ISCIII, Madrid, Spain. ⁸Department of Molecular and Integrative Physiology, University of Kansas Medical Center, Kansas City, KS, USA. ⁹Present address: Instituto de Investigaciones Químicas (IIQ-CICIC), CSIC-US, Seville, Spain. ¹⁰These authors contributed equally: Ismael Moreno-Sánchez, Luis Hernández-Huertas, Daniel Nahón-Cano. ✉ e-mail: mamormat@upo.es

that need to be addressed to further expand the in vivo capabilities of the CRISPR-RfxCas13d system.

First, targeting nuclear RNAs or zygotically expressed genes transcribed after gastrulation is less efficient¹⁰. A second limitation is that a subset of in vitro-transcribed (IVT) gRNAs, but not their chemically synthesized versions, can trigger toxic effects during embryogenesis. Thirdly, as described in mammalian cells^{23–26} and in other CRISPR-Cas systems both in vivo and ex vivo^{27–29}, on-target gRNA activity is variable and can challenge the targeting efficiency¹⁰. Moreover, CRISPR-RfxCas13d specificity has come under scrutiny lately due to the parallel and recent discoveries of collateral activity in eukaryotic cells^{30–36}. Collateral activity is a shared feature of all Cas13 family endonucleases and has been well established in bacteria and in vitro^{37–39}. It is defined as the cleavage of non-target RNAs that relies upon on-target gRNA recognition and stems from the three-dimensional structure of the two HEPN (Higher Eukaryotes and Prokaryotes Nucleotide-binding) nuclease domains in Cas13 family members. After the activation and a conformational change of Cas13, the HEPN domains are exposed on the outside of the protein and are able to cleave other accessible RNA molecules^{40,41}. In eukaryotes, this phenomenon has been mainly observed in ex vivo contexts such as mammalian or *Drosophila* cell cultures and/or when gRNAs and RfxCas13d are highly expressed from constitutive promoters^{30–36}. RfxCas13d collateral activity has yet to be characterized in vivo using transient targeting approaches (the delivery of RNP or mRNA-gRNA formulations) or assessed in the context of embryo development.

Here, we enhance RNA-targeting CRISPR-Cas technology in vivo through different and compatible approaches using zebrafish embryos as a model system. First, we show that chemically modified gRNAs (cm-gRNAs), along with *RfxCas13d* mRNA, significantly increase the loss-of-function phenotype penetrance when targeting mRNA from genes with late expression during development. Second, we implement an approach to select high-quality IVT gRNAs to avoid potential toxic effects in vivo. Third, we optimize RfxCas13d nuclear targeting along zebrafish early development by incorporating nuclear localization signals previously used to increase the activity of DNA-targeting CRISPR-Cas systems. Fourth, we compare different computational models recently developed in mammalian cell cultures^{24–26}, analyze their accuracy to predict the activity of 200 gRNAs delivered as RNP complexes, and define the most accurate approach for classifying CRISPR-RfxCas13d efficiency in vivo. Fifth, we demonstrate that transient CRISPR-RfxCas13d approaches can be used to deplete the vast majority of naturally present mRNAs in zebrafish embryos without inducing collateral activity, although this effect is triggered when targeting extremely abundant and ectopic mRNAs. Finally, we evaluate and compare the on-target and collateral activity of other RNA-targeting CRISPR-Cas systems, such as CRISPR-Cas7-11, CRISPR-DjCas13d and a high-fidelity version of RfxCas13d, formulated as RNP complexes. We demonstrate that CRISPR-Cas7-11 and specially CRISPR-DjCas13d can efficiently eliminate mRNAs in vivo and with absent or lower collateral effects than CRISPR-RfxCas13d respectively, when depleting highly abundant and ectopic RNAs in zebrafish embryos. Overall, our work constitutes a significant contribution towards better comprehension and enhancement of transient CRISPR-Cas approaches to target RNA in zebrafish embryos that will ultimately facilitate more effective integration of RNA-targeting CRISPR-Cas into in vivo KD-based biotechnological and biomedical applications.

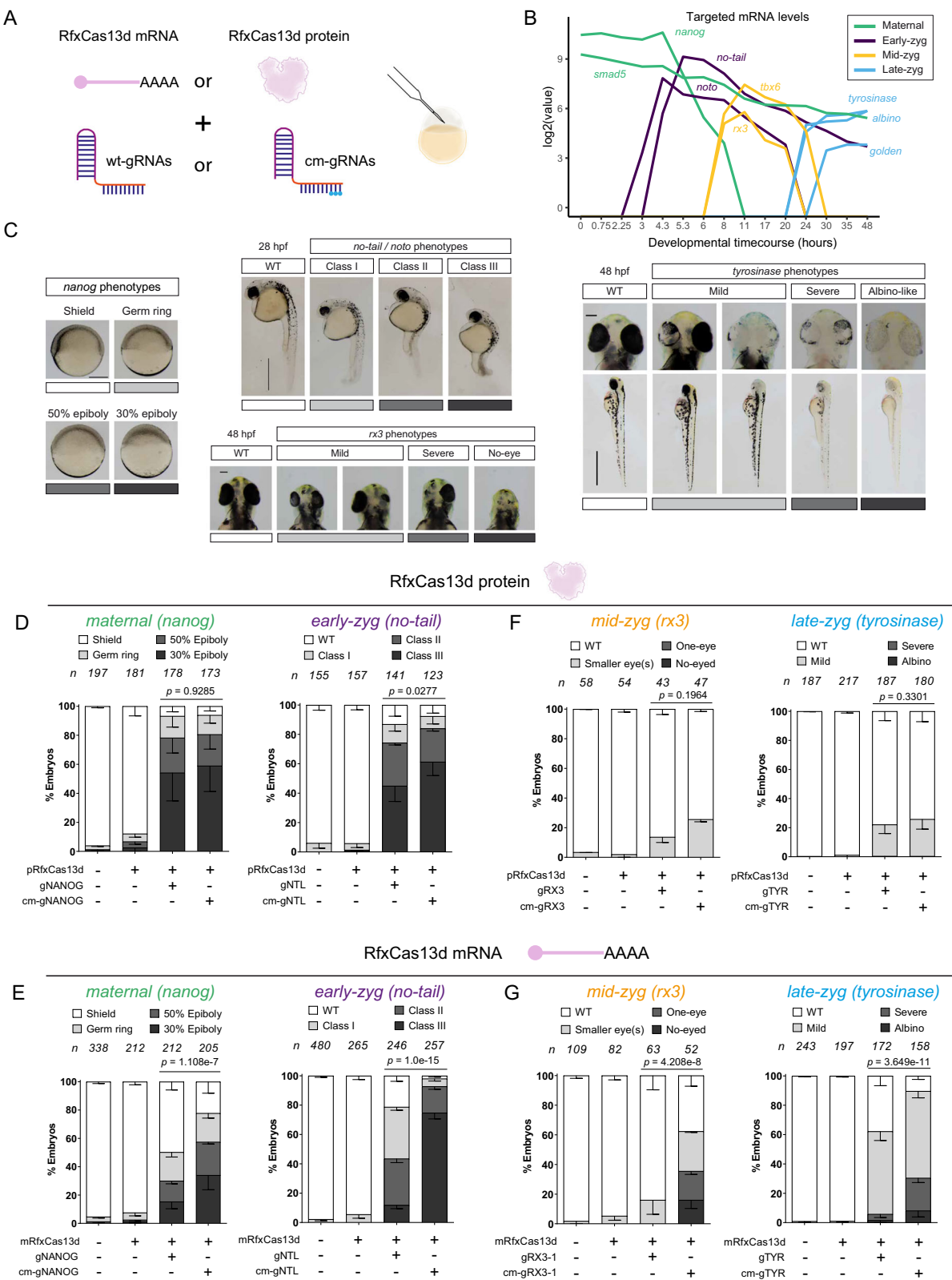
Results

CRISPR-RfxCas13d guide RNA optimizations lead to straightforward and sustained targeting in zebrafish embryos

CRISPR-RfxCas13d has shown high activity when targeting maternally provided and early transcribed mRNAs during vertebrate embryogenesis^{10–12,15–19,42}. However, the system performed with lower efficiency when depleting genes expressed after 7–8 hours

post-fertilization (hpf)¹⁰. Since cm-gRNAs have been used to maintain the efficiency of mRNA depletion in mammalian cell cultures⁴³, we hypothesized that this could be used during zebrafish embryogenesis to sustain and increase RNA targeting in vivo. We employed gRNAs with the most efficient chemical modification described in in vitro approaches (cm-gRNAs, 2'-O-methyl analogs and 3'-phosphorothioate internucleotide linkage in the last three nucleotides⁴³) combined with either mRNA or purified protein RfxCas13d (Fig. 1A). We targeted different maternally provided mRNAs and zygotically transcribed mRNAs in zebrafish embryos whose lack of function and therefore, phenotype penetrance could be easily visualized and quantified^{10,11,44} (Fig. 1B–G, Supplementary Fig. 1). For example, the KD of maternal *nanog* mRNA leads to epiboly defects with a substantial fraction of embryos at 30–50% epiboly at 6 hpf instead of germ ring or shield stage⁴⁵ (Fig. 1C) and *smad5* mRNA targeting induces a whole body dorsalization phenotype⁴⁶ (Supplementary Fig. 1A). The KDs of *tbxta* (hereafter named as *no-tail*) and *noto* mRNAs cause a reduction and/or the lack of the notochord and posterior part in the embryo⁴⁷ (Fig. 1C). In addition, the KD of *rx3* and *tbxt6* impairs eye development⁴⁸ and proper somite formation⁴⁹ respectively, and the KDs of *tyrosinase* (*tyr*), *slc45a2* (hereafter named as *albino*) and *slc24a5* (hereafter named as *golden*) mRNAs produce a loss of pigmentation²⁷ (Fig. 1C, Supplementary Fig. 1A). While maternally provided *nanog* and *smad5* mRNA were efficiently targeted by RNP complexes without any improvement using cm-gRNAs (Fig. 1D, Supplementary Fig. 1B, C), early zygotically expressed mRNAs (*no-tail* and *noto*) KD experienced a subtle but still significant increase in the phenotype penetrance (Fig. 1D, E, Supplementary Fig. 1B, C). Therefore, for these four maternally provided or early zygotically expressed genes whose highest mRNA levels are between 0 and 6 hpf, RNP complexes were more or equally efficient than the combination of *RfxCas13d* mRNA and gRNAs with or without chemical modifications (Fig. 1D, E, Supplementary Fig. 1B, C). Conversely, independently of the use of cm-gRNAs, RNP complexes were much less active when targeting mRNAs expressed from five genes whose main expression occurs after 7–8 hpf, i.e., *rx3*, *tbxt6*, *tyrosinase*, *albino*, and *golden* (mid- or late-zygotically transcribed genes, Fig. 1B, F, Supplementary Fig. 1B). Notably, the combination of *RfxCas13d* mRNA and cm-gRNA showed a superior efficiency eliminating mRNAs from mid- or late-zygotically transcribed genes with a more penetrant phenotype and robust targeting outperforming the use of RNP complexes (Fig. 1F, G, Supplementary Fig. 1B–D). Altogether, these results demonstrate that cm-gRNAs increase the activity of CRISPR-RfxCas13d on transcripts from genes expressed after 7–8 hpf during zebrafish embryogenesis and validate the use of cm-gRNA to deplete RNA in vivo. Additionally, we tested whether longer spacers (30 nucleotides, nt) might slightly boost RNA depletion in vivo by CRISPR-RfxCas13d as it was previously described in mammalian cell cultures²³. However, either 23 or 30 nt gRNAs led to a similar efficiency targeting maternal or zygotically expressed mRNAs with both RfxCas13d mRNA or protein (Supplementary Fig. 2).

In all previous experiments (Fig. 1 and Supplementary Figs. 1 and 2), we employed chemically synthesized and commercially available gRNAs (see “Methods”). Alternatively, efficient and specific gRNAs can be produced through oligo-annealing and fill-in PCR, followed by in vitro transcription (hereafter: IVT gRNAs)^{10,11}. Nevertheless, employing IVT gRNAs we have occasionally observed toxic effects in zebrafish embryos. For example, when targeting *si:dkcy-93m18.4* mRNA, a lowly expressed transcript, with three individual IVT gRNAs, we detected three distinct phenotypes when injected with RfxCas13d protein. While gRNA1 had no effect during embryogenesis, gRNA2 showed early embryogenesis delay, and gRNA3 revealed even earlier developmental defects that were observed by 2 hpf and with most of the embryos dead within the first 6 hpf (Fig. 2A,



Supplementary Fig. 3A). Conversely, targeting *si:dkey-93m18.4* mRNA with any of these three gRNAs showed comparably strong (>90%) KD at 4 hpf (Fig. 2B). We next wondered whether this toxic effect stemmed from in vitro transcription synthesis or was a direct result of gRNA sequence. To address this, we used chemically synthesized gRNA1 and gRNA3 targeting *si:dkey-93m18.4* mRNA. Injection of chemically synthesized gRNA1 produced no developmental effects, as expected. In

contrast to the lethality observed with IVTed gRNA3, embryos injected with chemically synthesized gRNA3 exhibited normal development (Fig. 2A, Supplementary Fig. 3A). Critically, RfxCas13d with chemically synthesized gRNAs achieved similar *si:dkey-93m18.4* KD to their IVTed counterparts (Fig. 2B). Taken together, this data demonstrates that a subset of RfxCas13d gRNAs can have toxic effects when produced by in vitro transcription.

Fig. 1 | Sustained CRISPR-RfxCas13d targeting in zebrafish embryos.

A Schematic illustration of the experimental setup used to compare CRISPR-RfxCas13d activity using standard (wt-gRNAs) or chemically modified (cm-gRNAs) gRNAs, with both mRNA (*RfxCas13d* mRNA) and purified protein (RfxCas13d protein). One-cell stage zebrafish embryos were injected with 300 pg of *RfxCas13d* mRNA or 3 ng of RfxCas13d protein together with 1 ng of a mix of three gRNAs (~300 pg/gRNA) (otherwise indicated in the corresponding figure legend). **B** Expression levels (log₂ TPM: Transcript per million reads) during the first 48 hours post-fertilization (hpf) of the different maternally provided (*nanog* and *smad5*) and zygotically expressed (*tbxta-no-tail*, *noto*, *rx3*, *tbx6*, *tyrosinase*, *slc45a2-albino*, and *slc24a5-golden*) mRNAs targeted in this study. Early-zyg, Mid-zyg and Late-zyg indicate early, mid, and late-zygotically expressed mRNAs, respectively. Data from zebrafish Expression Atlas⁴⁴. TPM values lower than 10 were referred to 0. **C** Representative images of the phenotypes obtained after the injection of the mRNA-gRNAs or ribonucleoprotein (RNP) complexes targeting the indicated maternally-provided or zygotically expressed mRNAs. *Nanog* loss-of-function phenotypes were evaluated at 6 hpf (scale bar, 0.25 mm). *Tbxta-no-tail* or

noto loss-of-function phenotypes were evaluated at 28 hpf (scale bar, 0.5 mm). *Rx3* (scale bar, 0.1 mm) and *tyrosinase* (scale bar, 0.75 mm for lateral views and 0.1 mm for insets) loss-of-function phenotypes were evaluated at 48 hpf. See “Methods” for a detailed description of loss-of-function phenotypes. Stacked barplots showing the percentage of observed phenotypes in zebrafish embryos injected with standard or cm-gRNAs targeting *nanog* (gNANOG) and *no-tail* (gNTL) together with RfxCas13d protein (pRfxCas13d, **D**) or mRNA (mRfxCas13d, **E**). Stacked barplots showing the percentage of observed phenotypes in zebrafish embryos injected with standard or cm-gRNAs targeting *rx3* (gRX3) and *tyrosinase* (gTYR) together with RfxCas13d protein (pRfxCas13d, **F**) or mRNA (mRfxCas13d, **G**). (*n*) total number of embryos is shown for each condition. The results are shown as the averages ± standard deviation of the mean of each phenotypic category. *p* value is indicated above. Statistical information is shown in Supplementary Data 1. Source data is provided as a Source Data file. Schematics adapted from Developmental Cell, Volume 54, Issue 6, Gopal Kushawah et al. CRISPR-Cas13d Induces Efficient mRNA Knockdown in Animal Embryos, 805–817.e7, Copyright (2020), with permission from Elsevier.

One of the molecular outcomes from these toxic effects was that, beyond the expected 18S and 28S ribosomal RNA (rRNA) observed in an RNA integrity analysis, we detected two prominent RNA species (Fig. 2C, Supplementary Fig. 3B) in *si:dkey-93m18.4* KDs consistently of ~1000 and ~2500 nucleotides (nt) in length and associated with developmental effects. We employed these two 28S rRNA cleavage species and their positions to ratiometrically quantify the integrity of the 28S rRNA. Controls and *si:dkey-93m18.4* KDs without developmental effects exhibited similar 28S integrity (Fig. 2D, E) whereas KDs with IVTed gRNA2 and gRNA3 showed significant decreases in 28S integrity that scale with both phenotype onset and severity (Fig. 2A, C–E, Supplementary Fig. 3A, B).

Correspondingly, we observed similar results when we targeted *brd4* mRNA using an IVTed or a chemically synthesized gRNA, both inducing a significant reduction of transcript levels (Fig. 2F, G). *Brd4* mRNA KD causes epiboly defects¹⁰ that were recapitulated by the chemically synthesized gRNA (Fig. 2F). However, the IVTed gRNA triggered a severe early embryogenesis lethality associated with a 28S rRNA fragmentation (Fig. 2F, H and Supplementary Fig. 3B).

Furthermore, we developed a simple in vitro rRNA integrity assay method to screen for IVTed gRNAs without a 28S rRNA cleavage effect associated with toxicity. We combined RfxCas13d protein, and/or gRNA with zebrafish total RNA and examined the total RNA through electrophoresis (Supplementary Fig. 3C). For example, in *si:dkey-93m18.4* KDs we observed that neither RfxCas13d alone nor gRNA1 or chemically synthesized gRNAs (1 and 3) as well as gRNAs alone (Supplementary Fig. 3D) had any substantial effect on the rRNA integrity in this assay. In contrast, RfxCas13d with IVTed gRNA2 and gRNA3 triggered rRNA cleavage in vitro (Supplementary Fig. 3D), which was more severe than that observed in total RNA from injected embryos (Supplementary Fig. 3B).

CRISPR-SpCas9 and CRISPR-Cas12a systems in mammalian cells can trigger cytotoxic effects via RIG-I and the interferon response due to the 5′ triphosphate in IVTed gRNAs that can be mitigated by 5′ phosphatase treatment (e.g. using calf-intestinal alkaline phosphatase, CIP)^{50,51}. However, while a deregulated transcriptome was associated with IVTed gRNAs inducing toxicity, RNAseq data did not show that interferon-related genes were upregulated in 4 hpf embryos co-injected with those gRNAs (Fig. 2I, J and Supplementary Fig. 3E). In addition, we observed that IVTed gRNAs pre-treated with CIP did not reduce the toxic effect observed in zebrafish embryos while they still showed high target efficacy (Fig. 2K, L and Supplementary Fig. 3F, G). Similar results were observed with gRNAs generated with T3 RNA polymerase (Supplementary Fig. 3H, I) suggesting that this toxicity triggered by some IVTed gRNAs did not depend on the RNA polymerase used in the in vitro reaction.

Altogether, these data demonstrated that some IVTed gRNAs for RfxCas13d may induce 28S rRNA fragmentation in vitro and in vivo that is associated with severe defects during embryogenesis and toxicity. These IVTed gRNAs do not induce an interferon response and their 5′ triphosphate end is not the trigger of the toxicity (Fig. 2I–L and Supplementary Fig. 3E–I). Importantly, these toxic effects can be overcome by (i) using chemically synthesized gRNAs or (ii) pre-screening IVTed gRNAs with our in vitro rRNA integrity assay.

Enhancing nuclear RNA depletion by CRISPR-RfxCas13d in zebrafish embryos

Efficient nuclear RNA targeting can be crucial to eliminate RNAs located in this cellular compartment, such as long non-coding RNAs or primary microRNAs^{52–54}. However, our optimized approach triggers mRNA KD in the cytosol. Indeed, a version of RfxCas13d with nuclear localization signals (NLS, RfxCas13d-NLS) was much less active in zebrafish embryos¹⁰ in contrast to what was observed in mammalian cell cultures when RfxCas13d targets the nascent mRNA¹. We hypothesized that the optimization of NLS could improve the efficacy of nuclear RNA elimination mediated by RfxCas13d in zebrafish embryos. We tested 4 NLS formulations that have been shown to increase nuclear-targeting effectiveness with CRISPR-Cas systems with DNA endonuclease activity^{55–58}. All NLS versions were innocuous during early zebrafish development when fused to RfxCas13d (Supplementary Fig. 4). We observed that 2 NLS (SV40-Nucleoplasmin long NLS) at the carboxy-terminus⁵⁵ of RfxCas13d (RfxCas13d-2C-NLS) significantly caused the highest phenotype penetrance observed at 48 hpf when targeting the primary and nuclear transcript of miR-430 (pri-miR-430) (Fig. 3A, B and Supplementary Fig. 4), a microRNA involved in early development regulation that eliminate hundreds of mRNAs during the first hours of development^{59–61}. Indeed, we performed a transcriptomic analysis and observed that this pri-miR-430 targeting induced by RfxCas13d-2C-NLS, specifically triggered a global stabilization of a subset of 203 maternal mRNAs whose degradation was more strictly dependent on miR-430^{62,63} (Fig. 3C). Notably, this stabilization only affected to this group of mRNAs without any substantial alteration of other maternal mRNA decay programs depending on other maternally provided or zygotically expressed factors⁶³, suggesting a specific effect on miR-430-dependent mRNA decay (Fig. 3C). Furthermore, RfxCas13d-2C-NLS version induced a significant reduction of primary and, consequently, mature miR-430 levels analyzed by qRT-PCR that was not observed when cytosolic RfxCas13d or a non-optimal RfxCas13d-NLS¹⁰ were used (Fig. 3D, E). Notably, despite the intrinsic mosaicism of the microinjection, pri-miR-430 KD phenotype at 48 hpf was partially rescued by a mature version of miR-430 (Fig. 3F). This set of results strongly suggests that observed developmental defects were specifically caused by the primary miR-430 targeting and

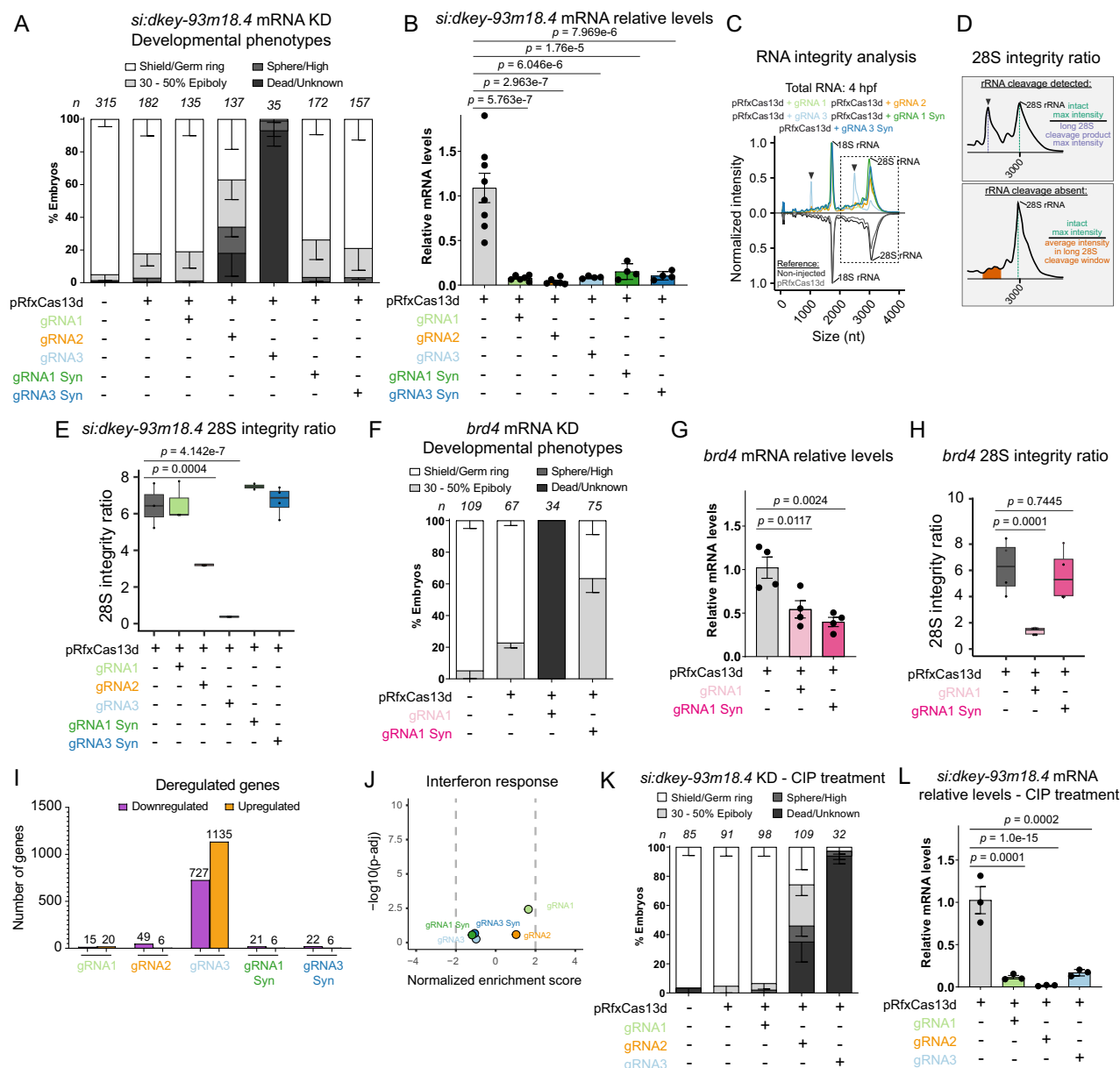
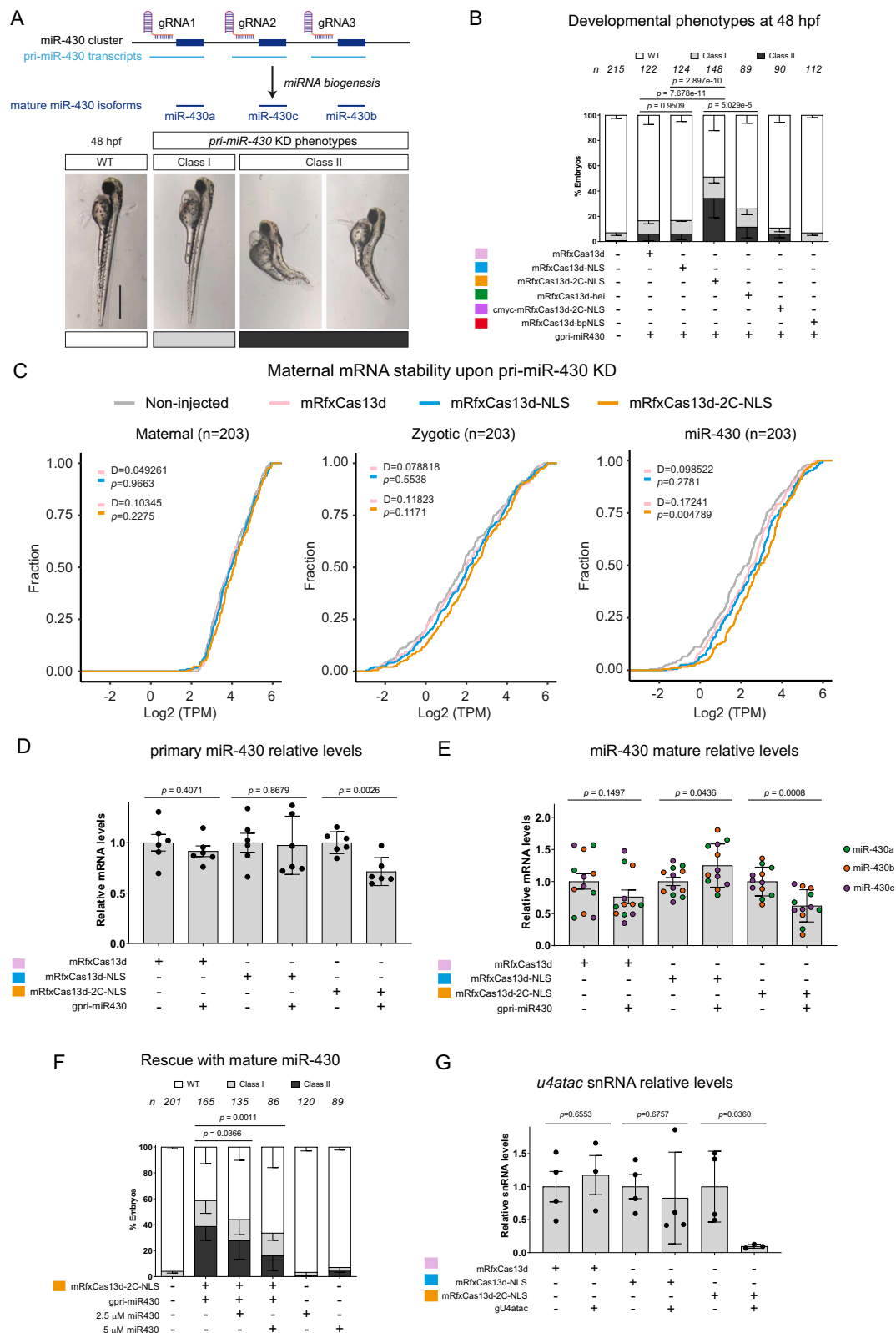


Fig. 2 | In vitro-transcribed gRNAs can induce toxicity. A Stacked barplots showing the percentage of developmental effect of *si:dkey-93m18.4* KD at 6 hpf using in vitro-transcribed gRNAs (IVTed, gRNAs 1–3) or chemically synthesized (Syn, gRNAs 1 and 3) gRNAs (400 pg/embryo). **B** Barplot showing relative *si:dkey-93m18.4* mRNA levels measured by qRT-PCR at 4 hpf from injected embryos in (A). *cdk2ap2* mRNA was used as a normalization control. **C** Mirrored line-plot represents relative abundance (normalized fluorescence intensity of bioanalyzer electrophoresis) of RNA species present in total RNA at 4 hpf from RfxCas13d mediated *si:dkey-93m18.4* KD and control embryos. Traces are single replicates. Non-injected (gray) and RfxCas13d alone (black) traces are inverted as a reference for RfxCas13d + gRNA1 (light green), RfxCas13d + gRNA2 (orange), RfxCas13d + gRNA3 (light blue), RfxCas13d + gRNA1 Syn (dark green), and RfxCas13d + gRNA3 Syn (dark blue). Black arrows denote peaks from 28S rRNA cleavage. **D** Cartoon of 28S integrity ratio calculation as the intensity of the 28S rRNA relative to the long 28S cleavage product when detected (top) and when it was absent (bottom). **E** Boxplot of 28S integrity ratio in vivo at 4 hpf from RfxCas13d mediated *si:dkey-93m18.4* KD and control embryos. **F** Stacked barplots showing the percentage of developmental phenotypes upon *brd4* mRNA KD at 6 hpf using an in vitro-transcribed or chemically synthesized gRNA (IVTed, gRNA1, and Syn, respectively; 300 pg of gRNA/embryo). **G** Barplots showing relative *brd4* mRNA levels measured by qRT-PCR at 4 hpf from injected embryos in (F). *tafl5* mRNA was used as a normalization control.

H Boxplot of 28S integrity ratio in vivo at 4 hpf from (F). **I** Number of down- (purple) and upregulated (orange) genes analyzed by RNAseq in injected embryos with RfxCas13d together with IVTed and chemically synthesized gRNAs targeting *si:dkey-93m18.4*. Fold Change of 2 and p value < 0.001 were used to determine deregulated genes. **J** Scatter plot of Normalized Enrichment Score and adjusted p value associated with Gene Set Enrichment analysis of interferon response genes⁹⁴. Bulk-RNA-Seq data from (I) and Supplementary Fig. 3. Vertical dashed lines indicate -2 and 2 Normalized Enrichment Score. **K** Stacked barplots showing the percentage of developmental effect of *si:dkey-93m18.4* KD at 6 hpf using in vitro-transcribed gRNAs (IVTed, gRNAs 1–3) after CIP treatment (400 pg/embryo). **L** Barplots showing relative *si:dkey-93m18.4* mRNA levels measured by qRT-PCR at 4 hpf from injected embryos in (K). *cdk2ap2* mRNA was used as a normalization control. The phenotypic results are shown as the averages \pm standard deviation of the mean of each developmental stage (A, F, K). mRNA relative levels measured by qRT-PCR are shown as the averages \pm standard deviation of the mean (B, G, L). Individual values are represented by points in boxplots (E, H). The mean, first, and third quartile are represented for each condition. Vertical lines indicate the variability outside the upper and lower quartiles. p values are indicated above. Statistical information is shown in Supplementary Data 1. Source data is provided as a Source Data file.



loss-of-function. In addition, the optimized RfxCas13d-2C-NLS also triggered efficient and significant KD of a small nuclear RNA, *u4atac* snRNA⁶⁴, that was not depleted by cytosolic RfxCas13d or our previous RfxCas13d-NLS¹⁰ (Fig. 3F).

Altogether, our results demonstrate that CRISPR-RfxCas13d-2C-NLS system used as a mRNA-gRNA formulation efficiently depletes nuclear RNAs in zebrafish embryos.

RNA targeting, an ex vivo-based computational model, can moderately predict CRISPR-RfxCas13d activity in vivo

Several computational models have been recently developed to predict CRISPR-RfxCas13d activity^{23–26}. These models were based on data where RfxCas13d and gRNAs were expressed from constitutive promoters in mammalian cell cultures^{23–26}. However, in vivo, approaches frequently imply the delivery of a purified RfxCas13d protein or

Fig. 3 | An optimized localization signal enhances CRISPR-RfxCas13d nuclear RNA-targeting. **A** Diagram (top) illustrating the locations of gRNAs designed within pri-miR-430 transcript (light blue lines) without targeting pre-miR-430 or mature miR-430a/b/c isoforms⁶¹ (dark blue rectangles). Representative images of developmental defects observed at 48 hpf upon pri-miR-430 (scale bar, 0.75 mm) (bottom). Class I: heart edema (mild phenotype); Class II: body curvature and/or tail blister (severe phenotype). **B** Stacked barplots showing the percentage of phenotypes at 48 hpf comparing cytoplasmic (mRfxCas13d, pink) and nuclear RfxCas13d mRNA versions (mRfxCas13d-NLS, blue; mRfxCas13d-2C-NLS, orange; mRfxCas13d-hei, green; cmRfxCas13d-2C-NLS, purple; mRfxCas13d-bpNLS, red) targeting pri-miR-430 (gpri-miR-430). The design of the different NLS versions is shown in Supplementary Fig. 4A and detailed in “Methods”. **C** Cumulative plot of the mRNA levels degraded by maternal, zygotic, and miR-430 pathways (maternal, zygotic, and miR-430) through early zebrafish development^{62,63} in control (Non-injected; gray line), and different pri-miR-430 KD conditions using mRfxCas13d, mRfxCas13d-NLS or mRfxCas13d-2C-NLS (see **B**). mRNAs controlled by miR-430 and 203 random mRNAs (*n*) degraded by maternal and zygotic pathways^{62,63} were analyzed and the maximal vertical distance between compared distributions (**D**) is shown. **D** Barplots showing primary miR-430 relative levels measured by qRT-PCR at 5 hpf using mRfxCas13d, mRfxCas13d-NLS, and mRfxCas13d-2C-NLS and gRNAs

from (**A**) *taf15* was used as a normalization control. **E** Barplots showing relative levels of three miR-430 mature isoforms (miR-430a, miR-430b, and miR-430c: green, orange, and purple dots, respectively) from the conditions in (**D**) *u4atac* snRNA was used as a normalization control. **F** Stacked barplots showing the percentage of observed phenotypes at 48 hpf upon pri-miR-430 targeting using mRfxCas13d-2C-NLS and co-injected with 1 nL of exogenous mature-miR-430 at different concentrations. **G** Barplots showing snRNA *u4atac* relative levels measured by qRT-PCR at 6 hpf using mRfxCas13d, mRfxCas13d-NLS, and mRfxCas13d-2C-NLS and gRNAs. miR-430b was used as a normalization control. (*n*) total number of injected embryos is shown for each condition. The results are shown as the averages \pm standard deviation of the mean of each phenotypic category (**B**, **F**). Two-sided χ^2 statistical test was performed to indicate comparisons. mRNA relative levels measured by qRT-PCR are shown as the averages \pm standard deviation of the mean (**D**, **E**, **G**). A two-sided *t*-test statistical analysis was performed to compare control vs KD. *p* values are indicated above. Statistical information is shown in Supplementary Data 1. Source data is provided as a Source Data file. Schematics adapted from Developmental Cell, Volume 54, Issue 6, Gopal Kushawah et al. CRISPR-Cas13d Induces Efficient mRNA Knockdown in Animal Embryos, 805–817.e7, Copyright (2020), with permission from Elsevier.

RfxCas13d mRNA and chemically synthesized or IVTed gRNAs. To examine whether computational models based on cell culture data were able to accurately predict CRISPR-RfxCas13d activity in vivo, we measured the efficiency of ~200 gRNAs in zebrafish embryos using our optimized and transient approach based on RNP complexes. First, to define the maximal number of gRNAs that could be used at the same time in zebrafish embryos allowing a successful detection of highly active gRNAs, we co-injected 10 and 25 gRNAs as optimal and sub-optimal targeting conditions (100 pg and 40 pg of gRNA per embryo, respectively) (Supplementary Fig. 5A, B). Next, we generated gRNA quintiles (q) based on their activity and observed that using up to 25 gRNAs injected together allowed us to detect highly efficient gRNAs (q4 and q5, respectively) previously identified in optimal conditions (Supplementary Fig. 5, fold change > 3.5, q4 and q5). Consequently, to reduce the number of injections and the economic cost of transcriptomics, we used sets of 25 gRNAs for further analysis. Thus, we injected eight independent combinations (gRNA set 1 to 8) of 25 gRNAs to KD 75 mRNAs (2–3 gRNAs per transcript) with high-moderate and stable levels between 1 and 4 hpf, where most of the targeting likely occurs (Fig. 4A, Supplementary Fig. 5C). Then, we performed an RNAseq analysis of each gRNA set at 4 hpf (Supplementary Fig. 6A, B) and analyzed the efficiency of those gRNAs (*n* = 191) whose activity could be predicted by the most recent and updated computational CRISPR-RfxCas13d models based on the activity of hundreds of thousands constitutively expressed gRNAs in mammalian cell culture^{24–26} (Fig. 4A and see “Methods” for details). Among the assessed models, RNAtargeting²⁶ was the most accurate in classifying CRISPR-RfxCas13d RNP complexes activity in zebrafish embryos (Fig. 4B, Supplementary Fig. 6C). Indeed, RNAtargeting was able to classify five out of eight sets of gRNAs with a similar or even more accuracy than what was calculated for an independent ex vivo data used as control (Cell culture data, Pearson’s correlation coefficient *R* > 0.38, Fig. 4B). Furthermore, RNAtargeting was the most efficient computational model distinguishing highly (top 5 per set) from poorly (bottom 5 per set) active gRNAs (Fig. 4C–E). These results suggest that RNAtargeting is the most useful current tool to select competent gRNAs. Nevertheless, RNA-targeting was less accurate at predicting CRISPR-RfxCas13d RNP activity in three out of eight sets, especially in one of them where there was not a positive correlation between the predicted scores and in vivo activity (Fig. 4B; gRNA set 7, Pearson’s correlation coefficient *R* = −0.05). Then, to further analyze this lower correlation between RNAtargeting prediction and CRISPR-RfxCas13d activity in vivo for those sets of gRNAs, we individually examined the most and less efficient gRNAs (top and bottom 5, respectively) per group

(Supplementary Fig. 6D–F). Despite this lower accuracy in the activity prediction for three out of eight sets of gRNAs, RNAtargeting still detected one gRNA from set 8 and set 5 as highly efficient (i.e., gRNAs with a score above the first quartile of highly active gRNAs selected by this algorithm in vivo; Score > 0.55, Supplementary Fig. 6D–F). However, highly active gRNAs from set 7, with the poorest Pearson correlation coefficient, failed to be detected by RNAtargeting. In addition, analyzing gRNAs with the lowest activity we also observed how in set 7, one gRNA was predicted as highly efficient by RNAtargeting (Score > 0.55, Supplementary Fig. 6D–F), suggesting that the lack of correlation of this set came from the poor prediction accuracy for both high and low active gRNAs. Together, our results validate the use of RNA-targeting to classify CRISPR-RfxCas13d system activity delivered in vivo as RNP complexes, yet with a modest level of accuracy.

Minimal collateral activity targeting endogenous mRNAs by CRISPR-RfxCas13d

The recently described collateral activity triggered by CRISPR-RfxCas13d in mammalian systems induces different molecular outcomes that can be used as hallmarks of this effect. The main consequence of this effect is the uncontrolled elimination of RNAs after the specific and initial targeting of both exogenous and endogenous transcripts^{32–36}. Besides, CRISPR-RfxCas13d-induced collateral activity is most severe when targeting highly expressed genes and ultimately causes cell toxicity, a decrease in cell proliferation^{32,33,36} and the cleavage of the 28S rRNA^{33,36}. First, and despite that, we did not clearly detect any of these effects when previously using our optimized RNP or mRNA-gRNA injections targeting endogenous or ectopic mRNAs^{10–12}, we sought to investigate the collateral activity when CRISPR-RfxCas13d system targeted a highly concentrated reporter (green fluorescent protein, GFP) mRNA injected in one-cell stage zebrafish embryos. We observed that, for different amounts (from 10 to 100 pg per embryo) of target, CRISPR-RfxCas13d efficiently depleted both mRNA and GFP protein (Fig. 5A–D). Notably, embryos injected with more than 50 pg of *gfp* mRNA experienced epiboly defects at 6 hpf (Fig. 5E, 30–50% epiboly) when using CRISPR-RfxCas13d as a mRNA-gRNA complex. This effect was more severe when using RNP complexes and, indeed, the KD of *gfp* mRNA injected at 20 or more pg per embryo triggered not only embryogenesis deficiencies but also an arrest during early development and death with the highest concentrations (100 pg per embryo caused a massive embryo death, *n* = 107 embryos from two independent experiments) (Fig. 5F). Moreover, we observed a cleavage of the 28S rRNA subunit in zebrafish embryos under these conditions correlating with a reduced RNA

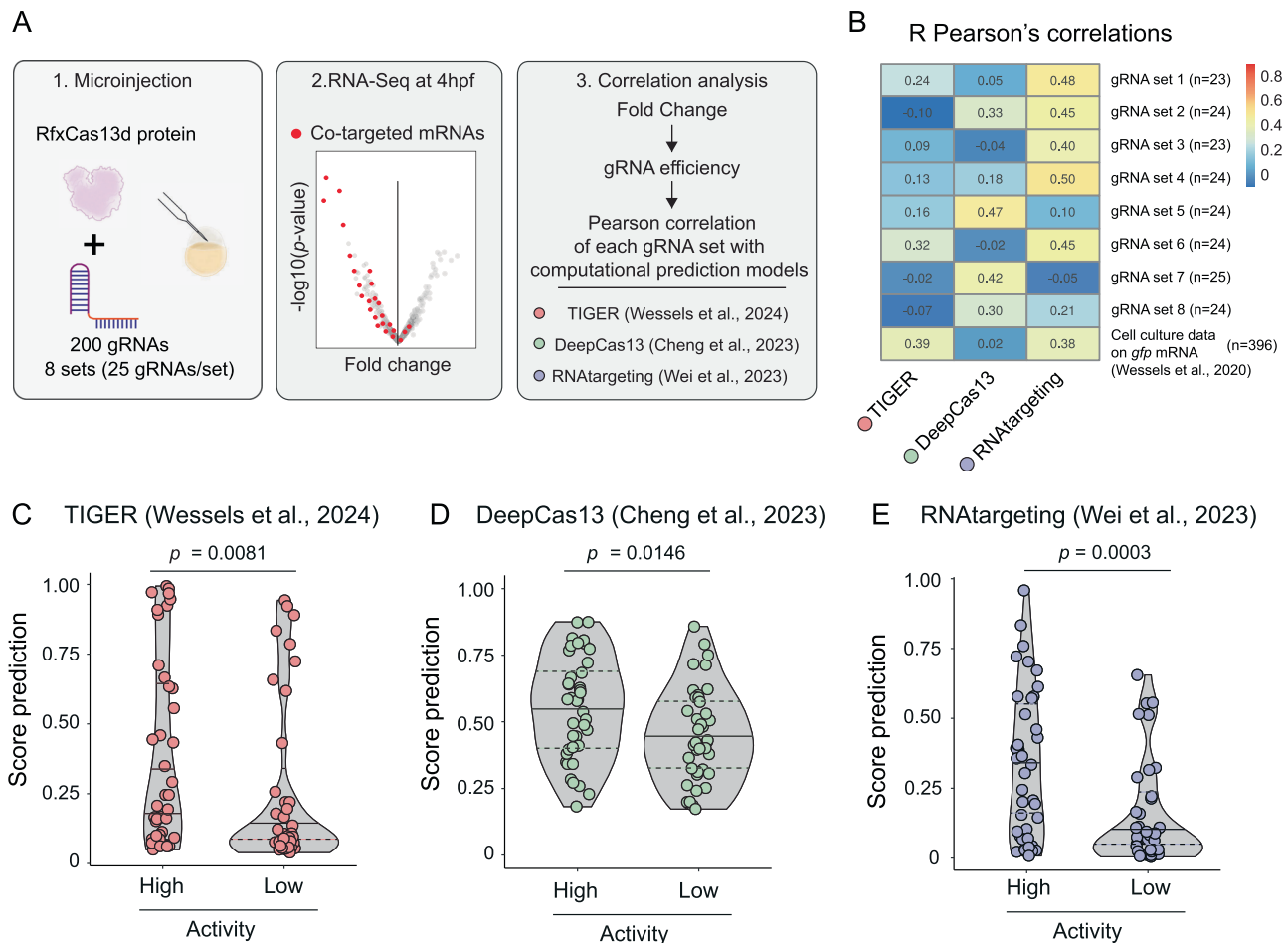


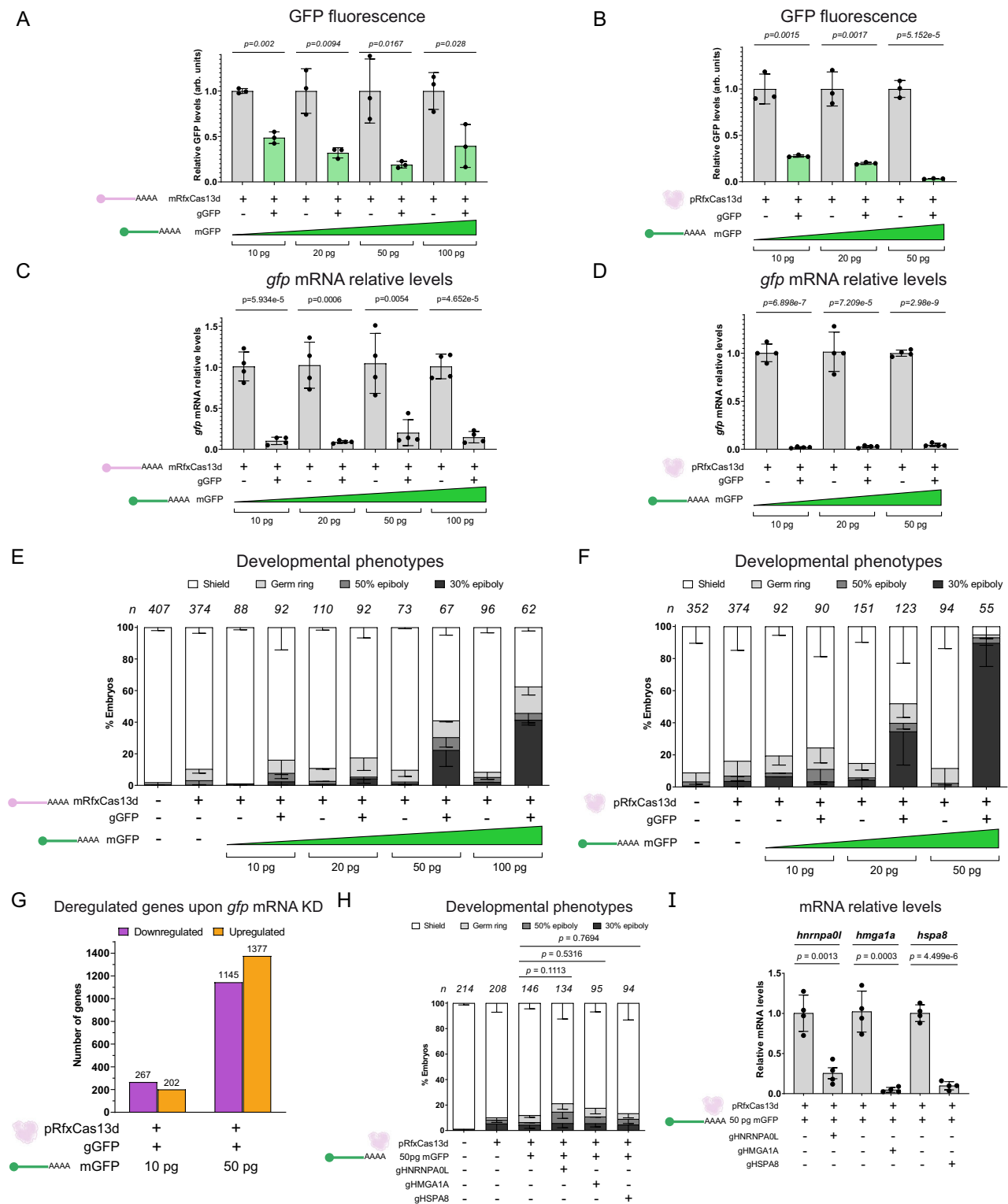
Fig. 4 | RNA-targeting, an ex vivo-based computational model can moderately predict CRISPR-RfxCas13d activity in vivo. **A** Workflow to assess the efficiency of computational models based on ex vivo data to predict in vivo activity. (1) Diagram illustrating the injection of 8 different sets of 25 gRNAs together with RfxCas13d protein in one-cell stage zebrafish embryos. (2) RNAseq was performed from injected embryos at 4 hpf. Co-targeted mRNAs per set are depicted in red. (3) Fold changes obtained from RNAseq data were used to calculate each gRNA efficiency and this was employed to calculate Pearson correlation with scores obtained from the most recent and updated computational prediction models based on ex vivo data^{24–26}. **B** Heatmap of Pearson's correlations coefficient from each gRNA set with scores predicted by computational models in (A): TIGER²⁴, red dots; DeepCas13²⁵,

green dots; RNAtargeting²⁶, purple dots. Pearson's correlation coefficient per computational model from cell culture data on *gfp* mRNA targeting using 396 gRNAs is included as a reference control (Wessels et al.²³). Violin-plots representing the score of the five highest (High) and five lowest (Low) active gRNAs per set predicted by TIGER²⁴ (C), DeepCas13²⁵ (D), and RNAtargeting²⁶ (E). The median and first and third quartiles of the 40 gRNAs score are represented as dashed and dotted lines, respectively. Statistical information is shown in Supplementary Data 1. Source data is provided as a Source Data file. Schematics adapted from Developmental Cell, Volume 54, Issue 6, Gopal Kushawah et al. CRISPR-Cas13d Induces Efficient mRNA Knockdown in Animal Embryos, 805–817.e7, Copyright (2020), with permission from Elsevier.

integrative number (RIN) (Supplementary Fig. 7A–C). Interestingly, even with the lowest concentration of *gfp* mRNA (10 pg per embryo), where no developmental delay was noticed upon KD, a notable 28S rRNA fragmentation could be visualized. This result suggests that RNA integrity assay was highly sensitive when detecting the collateral activity induced by CRISPR-RfxCas13d (Supplementary Fig. 7A, B). Further, when a red fluorescent protein (DsRed) mRNA was co-injected together with CRISPR-RfxCas13d RNP targeting *gfp* mRNA, the fluorescence of both reporters decreased (except with the lowest concentration of *gfp* mRNA where DsRed fluorescence was intact), although the developmental and molecular (28S rRNA fragmentation) effects were less severe (Supplementary Fig. 7D–G). This could likely be due to a buffer capacity from the *dsred* mRNA that, at high concentration, could partially alleviate the consequences of the collateral activity. To further understand the molecular consequences of the collateral activity during zebrafish embryogenesis, we performed a transcriptome analysis. We observed a global deregulation, especially when targeting an extremely abundant amount of *gfp* mRNA (50 pg/embryo), with 1145 downregulated and 1377 upregulated genes

(Fig. 5G, Supplementary Fig. 7H). This correlates with the developmental defects and 28S rRNA fragmentation previously observed. Together, our results demonstrate that RfxCas13d can trigger collateral activity upon the targeting of highly abundant reporter mRNAs.

Next, we sought to analyze whether the collateral activity could be detected when targeting endogenous mRNAs. We selected 3 maternally provided transcripts in zebrafish embryos, all above the top 25 most abundant mRNAs among the polyadenylated mRNAs during the first 6 hpf (Supplementary Fig. 8A). When we targeted these mRNAs, we did not observe any developmental defect despite triggering a significant depletion of these endogenous mRNAs (between 75–95% mRNA reduction) (Fig. 5H, I). In addition, we did not notice any collateral downregulation of GFP fluorescence from its mRNA that was co-injected together with RNP complexes targeting these endogenous mRNAs (Supplementary Fig. 8B). Interestingly, for the depleted endogenous targets, we detected a weak 28S rRNA fragmentation that was much less prominent than what was observed when targeting the lowest tested amount of *gfp* mRNA (Supplementary Figs. 7A, B and 8C). Nevertheless, this 28S rRNA fragmentation was still substantial when



rRNA 28S integrity ratio was analyzed (Fig. 2D and Supplementary Fig. 8D). This result indicates a minor collateral effect yet without any significant physiological consequence (Fig. 5H). Notably, we observed similar results when these endogenous mRNAs were targeted by CRISPR-RfxCas13d RNP complexes without *gfp* mRNA, suggesting that the presence of this transcript did not influence or buffer the collateral effects in these conditions (Supplementary Fig. 8E–G). Altogether, our results suggest that the collateral activity from CRISPR-RfxCas13d used as RNP or mRNA-gRNA complexes is minimal and without a physiological relevance even when targeting highly abundant mRNAs during

zebrafish embryogenesis. Nonetheless, it can be triggered when extremely expressed and ectopic transcripts such as injected reporters are targeted.

Implementation of alternative CRISPR-Cas systems for transient RNA-targeting in vivo

Although minimal when targeting endogenous mRNAs, the collateral activity induced by RfxCas13d can still be an issue under certain circumstances in vivo. For example, the use of RNA-targeting CRISPR-Cas technology as a potential therapeutic application driven by transient

Fig. 5 | CRISPR-RfxCas13d exhibits physiologically relevant collateral activity only when targeting extremely abundant ectopic mRNAs in zebrafish embryos.

Barplots showing GFP fluorescence levels of injected embryos with *RfxCas13d* mRNA (mRfxCas13d), (A) or RfxCas13d protein (pRfxCas13d), (B) together with gRNAs (gGFP) targeting increasing quantities of ectopic *gfp* mRNA (mGFP). Barplots showing *gfp* mRNA relative levels analyzed by qPCR of injected embryos with mRfxCas13d (C) or pRfxCas13d (D) together with gGFP targeting increasing quantities of ectopic mGFP. *taf15* mRNA was used as a normalization control. Stacked barplots representing developmental phenotypes (epiboly stages) of injected embryos with mRfxCas13d (E) or pRfxCas13d (F) together with gGFP targeting increasing quantities of ectopic mGFP. G Number of down- (purple) and upregulated (orange) genes from injected embryos with pRfxCas13d together with gGFP and 10 or 50 pg of mGFP. Fold Change of 2 and p value < 0.001 were set to determine deregulated genes. H Stacked barplots representing developmental phenotypes (epiboly stages) of injected embryos with pRfxCas13d together with 50 pg of mGFP as reporter for collateral activity and gRNAs targeting endogenous *hnrnpa0l*,

hmg1a and *hspa8* transcripts (gHNRNPA0L, gHMGA1A, and gHSPA8, respectively). I Barplots showing mRNA relative levels analyzed by qRT-PCR at 6 hpf of injected embryos with pRfxCas13d together with 50 pg of mGFP as reporter for collateral activity and gHNRNPA0L, gHMGA1A or gHSPA8. *taf15* mRNA was used as a normalization control. GFP fluorescence levels are shown as the averages \pm standard deviation of the mean (A, B). mRNA relative levels measured by qRT-PCR are shown as the averages \pm standard deviation of the mean (C, D, I). (n) total number of injected embryos is displayed for each condition. The phenotypic results are shown as the averages \pm standard deviation of the mean of each developmental stage (E, F, H). Representative images of indicated epiboly stages are shown in Fig. 1C. p values are indicated above. Statistical information is shown in Supplementary Data 1. Source data is provided as a Source Data file. Schematics adapted from Developmental Cell, Volume 54, Issue 6, Gopal Kushawah et al. CRISPR-Cas13d Induces Efficient mRNA Knockdown in Animal Embryos, 805–817.e7, Copyright (2020), with permission from Elsevier.

approaches needs to ensure a biosafety method where the collateral activity should be minimized or totally absent. Thus, we sought to optimize other RNA-targeting CRISPR-Cas systems in vivo that have recently shown little or no collateral activity while preserving high on-target efficacy when expressed from constitutive and strong promoters in mammalian cells: a high-fidelity version of CRISPR-RfxCas13d (Hf-RfxCas13d³²), CRISPR-Cas7-11⁶⁵ and CRISPR-DjCas13d²⁶. First, we purified these Cas proteins and tested them in zebrafish embryos. None of the proteins showed a substantial toxicity when injected alone (Fig. 6A and Supplementary Fig. 9A). Second, we used these Cas proteins to target *no-tail* and *nanog* using 1 and 3 gRNAs per mRNA, respectively. To analyze the efficiency of these systems compared with CRISPR-RfxCas13d, we quantified the phenotype penetrance upon the KD of *nanog* and *no-tail*. While DjCas13d induced a similar phenotype penetrance to RfxCas13d, Hf-RfxCas13d was much less efficient not only when injected as purified protein but also as mRNA (Fig. 6A–C, Supplementary Fig. 9B–D), suggesting that this endonuclease, transiently delivered as RNP or mRNA-gRNA complexes, is not highly competent to target mRNA in vivo. Further, CRISPR-Cas7-11 recapitulated the expected phenotype from the lack-of-function of *nanog* and *no-tail* with a slightly lower activity than CRISPR-Cas13d systems (Fig. 6A–C). Third, we quantified the mRNA levels of *nanog*, *no-tail*, and three highly abundant endogenous transcripts (*hnrnpa0l*, *hmg1a*, *hspa8*) formerly analyzed using RfxCas13d (Fig. 5H, I, Supplementary Fig. 8E, F) and targeted now by Hf-RfxCas13d, DjCas13d, and Cas7-11. Our results validated our previous data based on phenotype analysis (Fig. 6A–D, Supplementary Fig. 9B, C), and confirmed that Hf-RfxCas13d showed the lowest efficacy in vivo (42.2% average depletion) followed by Cas7-11 (60.1%) and DjCas13d (83.2%) that triggered an efficient mRNA depletion comparable to RfxCas13d activity (80.1%) (Fig. 6E–I). Next, we investigated whether DjCas13d and Cas7-11 showed collateral activity in zebrafish embryos using our previously defined non-physiological conditions that allow us to measure this effect employing reporter mRNAs. When targeting injected *gfp* mRNA, DjCas13d displayed less severe developmental defects than RfxCas13d. This toxicity increased with the concentration of the target, in agreement with what was observed previously for RfxCas13d in ex vivo and in vivo conditions^{32,33} (Fig. 6J, K, Supplementary Fig. 9E, G, I). Interestingly, and despite the developmental defects, the fragmentation of the 28S rRNA was not observed (Supplementary Fig. 9K), but we detected a non-specific down-regulation of DsRed fluorescence when its mRNA was co-injected with high amounts of *gfp* mRNA (Supplementary Fig. 10A–C). Notably, and as observed for RfxCas13d, the developmental phenotype triggered by *gfp* mRNA KD was mitigated when *dsred* mRNA was co-injected, suggesting a buffer effect that alleviates this alteration during embryogenesis (Fig. 6J, Supplementary Fig. 10A–C). In contrast, Cas7-11 did not show neither developmental defects nor 28S rRNA cleavage when

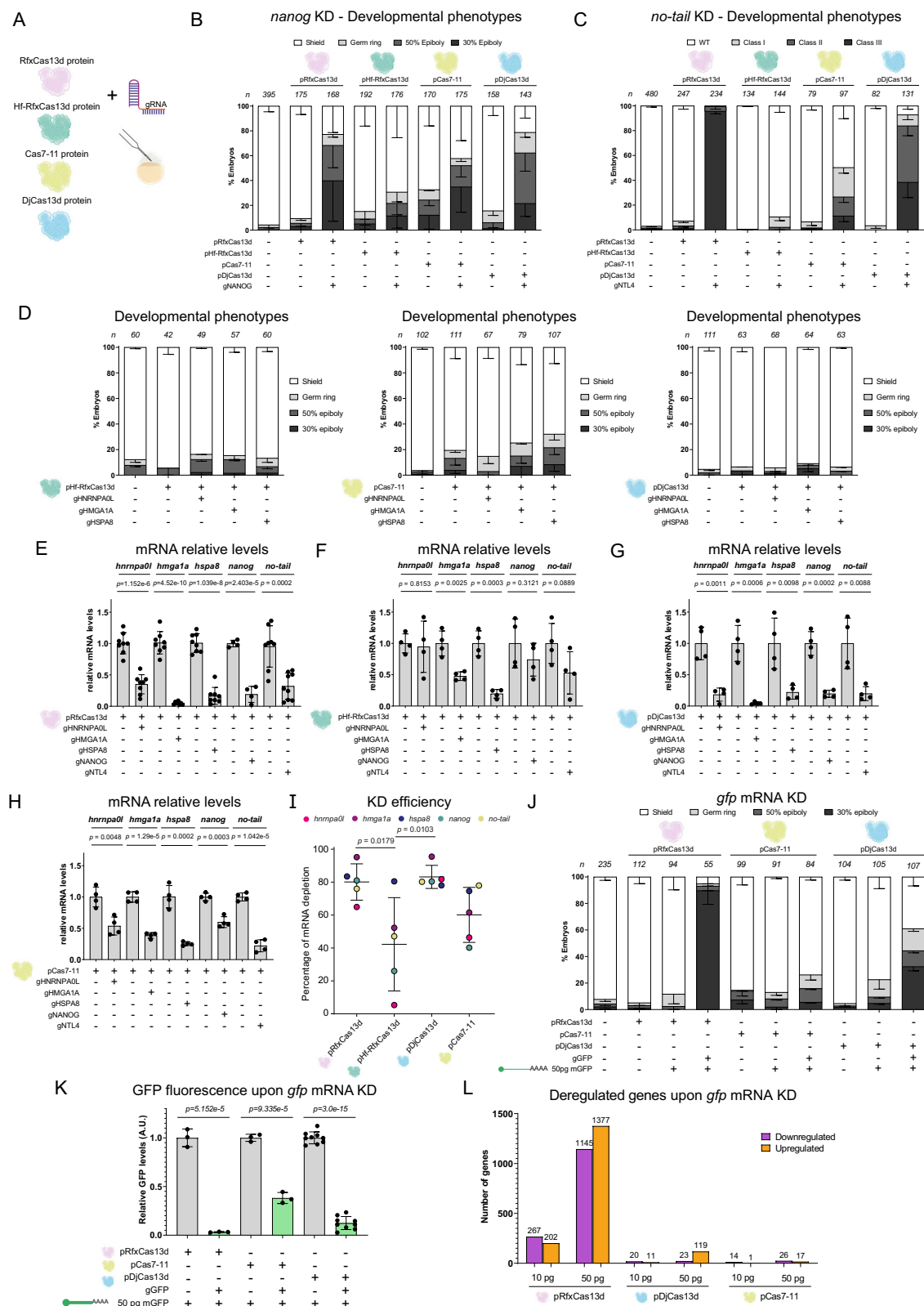
targeting *gfp* mRNA (Fig. 6J, K, Supplementary Fig. 9F, H, J, L). We also measured DsRed fluorescence when its mRNA was co-injected together with Cas7-11 RNP and *gfp* mRNA and we did not detect any significant decrease in protein activity (Supplementary Fig. 10D–F).

In addition, we performed a whole transcriptomic analysis and observed that while the *gfp* mRNA depletion was highly efficient using either RfxCas13d or DjCas13d (98.5% and 99.3% *gfp* mRNA depletion, respectively), the transcriptomic deregulation was strongly reduced when employing DjCas13d (a 98% and 91.4% reduction in number of downregulated and upregulated mRNAs in the most extreme condition: 50 pg *gfp* mRNA, Fig. 6L, Supplementary Fig. 11). Conversely, *gfp* mRNA depletion mediated by Cas7-11 did not trigger any significant transcriptomic alteration (Fig. 6L), but as previously shown (Fig. 6E–I), the efficiency of this endonuclease was lower than DjCas13d or RfxCas13d (Cas7-11: 76.5% *gfp* mRNA depletion, Supplementary Fig. 11). Since CRISPR-DjCas13d could be used alternatively to CRISPR-RfxCas13d with a similar on-target efficiency, we further explored whether the toxic effect induced by some IVT gRNAs for RfxCas13d could be also detected when employing CRISPR-DjCas13d system. Thus, we evaluated the toxicity of IVT gRNAs for DjCas13d. We used 3 similar IVT gRNAs that exhibited deleterious effects when using the CRISPR-RfxCas13d system and a control gRNA (Fig. 2 and Supplementary Fig. 3). Notably, none of these IVT gRNAs triggered cytotoxicity and recapitulated the expected developmental phenotypes observed when CRISPR-RfxCas13d and chemically synthesized gRNAs were employed. Furthermore, they showed a significant level of mRNA depletion comparable to their CRISPR-RfxCas13d gRNAs counterparts and to their chemically synthesized equivalents (Supplementary Fig. 12).

Together, our results (i) reaffirm that CRISPR-RfxCas13d is an efficient, specific and robust approach to target endogenous mRNA in zebrafish embryos and (ii) demonstrate that CRISPR-Cas7-11 and CRISPR-DjCas13d RNP can be used as alternative systems exhibiting a slightly lower or similar on-target activity than CRISPR-RfxCas13d and showing a total absence or reduced collateral effects when targeting extremely abundant ectopic RNAs, respectively.

Discussion

Our optimized CRISPR-RfxCas13d system has shown a high level of efficiency and specificity targeting maternal and early zygotically transcribed genes in zebrafish and other vertebrate embryos^{10–21}. Here, we have further enhanced CRISPR-Cas RNA-targeting in vivo using RNP and mRNA-gRNA formulations in zebrafish as a vertebrate model through different and complementary approaches. First, we have found that cm-gRNAs are able to maintain and increase the activity of CRISPR-RfxCas13d as described in human cells⁴³ especially depleting the expression of genes transcribed after 7–8 hpf where RNP complexes were less efficient. This may be due to a limited



half-life of RfxCas13d protein within the zebrafish embryos. Although DNA-targeting CRISPR-Cas systems can generate null alleles, this can obscure gene activities that can be compensated through transcriptional adaptation or only detected with a limited gene expression reduction^{66–68}. RfxCas13d together with cm-gRNAs allow us to titrate mRNA levels of the target enabling an alternative for these scenarios. Indeed, our optimized CRISPR-RfxCas13d system using

cm-gRNAs could contribute to widen the applications of combining transient perturbations with single-cell transcriptomics. This approach could allow to simultaneously associate the level of target depletion with a transcriptomic output at a single-cell level extending the use of this technology recently integrated with zebrafish crisprants or F0 mutant embryos targeted by DNA-targeting CRISPR-Cas approaches⁶⁹. Notably, cm-gRNAs have also been recently shown

Fig. 6 | Implementation of alternative CRISPR-Cas systems for transient RNA-targeting in vivo. **A** Schematic illustration of the experimental setup used to compare alternative and high-fidelity CRISPR-Cas RNA targeting systems (Hf-RfxCas13d³², DjCas13d²⁶, and Cas7-11⁶⁵) with CRISPR-RfxCas13d. One-cell stage zebrafish embryos were injected with 3 ng of each purified protein were injected together with 1 ng of a mix of three gRNAs (~300 pg/gRNA). Stacked barplots representing developmental phenotypes from injected embryos with RfxCas13d, Hf-RfxCas13d, Cas7-11, or DjCas13d together with three gRNAs targeting *nanog* (gNANOG, **B**) or one gRNA targeting *no-tail* (gNTL4, **C**). **D** Stacked barplots representing developmental phenotypes (epiboly stages) of injected embryos with Hf-RfxCas13d, Cas7-11, or DjCas13d together with gRNAs targeting endogenous *hnrnpa0l*, *hmg1a*, and *hspa8* transcripts (gHNRNPA0L, gHMG1A1, and gHSPA8, respectively). Barplots showing *nanog*, *tbxta*, *hnrnpa0l*, *hmg1a*, and *hspa8* mRNA levels analyzed from injected embryos with RfxCas13d (**E**), Hf-RfxCas13d (**F**), DjCas13d (**G**) or Cas7-11 (**H**) together with gHNRNPA0L, gHMG1A1, gHSPA8, gNANOG or gNTL4 analyzed by qRT-PCR at 4 (*nanog* and *tbxta*) or 6 hpf. **E** data corresponds to Fig. 5I and Supplementary Fig. 8F. *tafl5* mRNA was used as a normalization control. **I** Dot-blot showing KD efficiency of RfxCas13d, Hf-RfxCas13d, Cas7-11, and DjCas13d. Color dots represent the percentage of each

mRNA depletion from (**E–H**); mean and standard deviation are shown. **J** Stacked barplots representing developmental phenotypes (epiboly stages) of injected embryos with RfxCas13d, Cas7-11, or DjCas13d together with gRNAs targeting *gfp* (gGFP) and 50 pg of ectopic *gfp* mRNA (mGFP). **K** Barplots showing GFP fluorescence relative levels at 6 hpf from injected embryos in the conditions described in (**J**). **L** Number of down- (purple) and upregulated (orange) genes analyzed by RNAseq from injected embryos in the conditions described in (**J**). Fold Change of 2 and *p* value < 0.001 were used to determine deregulated genes. Deregulated genes shown for RfxCas13d are from Fig. 5G. Representative images of epiboly stages and *no-tail* phenotypes are shown in Fig. 1C. (*n*) total number of embryos is shown for each condition. The results are shown as the averages ± standard deviation of the mean of each developmental stage (**B–D, J**). mRNA relative levels measured by qRT-PCR (**E–H**) and GFP fluorescence levels (**K**) are shown as the averages ± standard deviation of the mean. *p* values are indicated above. Statistical information is shown in Supplementary Data 1. Source data is provided as a Source Data file. Schematics adapted from Developmental Cell, Volume 54, Issue 6, Gopal Kushawah et al. CRISPR-Cas13d Induces Efficient mRNA Knockdown in Animal Embryos, 805–817.e7, Copyright (2020), with permission from Elsevier.

to be useful in zebrafish RNA imaging, diversifying their applications in vivo²².

Second, we have increased nuclear RNA targeting throughout zebrafish embryogenesis using an enhanced NLS formulation. Indeed, we efficiently eliminated nuclear non-coding RNAs such as pri-miR-430 or a snRNA (*u4atac*). The incomplete maturity of the nuclear pore complexes during early zebrafish development that impairs nuclear protein import⁷⁰ can affect nuclear DNA or RNA targeting and our results suggest that this may be partially circumvented with an optimized NLS. Notably, this NLS was previously applied to enhance DNA targeting through Cas12a, not only in zebrafish embryos but also in mammalian cells⁵⁵, suggesting that it could be used to improve the nuclear RNA targeting of other CRISPR-Cas systems in different in vivo and ex vivo models.

Third, we have demonstrated that CRISPR-RfxCas13d RNP activity in vivo can be classified, and highly active gRNAs can be predicted by RNAtargeting, a computational model based on mammalian cell culture data, yet with a lower accuracy than shown for approaches using constitutive expression of both RfxCas13d and gRNA²⁶ (Fig. 4B). However, RNAtargeting is based on the activity from 127,000 gRNAs whose spacers were 30 nt long²⁶. Although we have shown that RNP activity in vivo is similar in employing gRNAs with either short (23 nt) or long (30 nt) spacers (Supplementary Fig. 2) and we have precisely adapted RNAtargeting to predict our data set based on short spacers (Fig. 4B and see “Methods” for details), we cannot rule out that the prediction of CRISPR-RfxCas13d RNP activity in vivo could be improved when using long spacers. Nevertheless, it has been previously reported that computational models predicting CRISPR-Cas DNA-targeting activity notably differ depending on the employed method. Thus, CRISPR-SpCas9 efficiency prediction models depend on whether the gRNA is constitutively transcribed from a U6 promoter or generated in vitro⁷¹. Indeed, RNAtargeting CRISPR-RfxCas13d prediction activity in vivo is limited and failed to accurately classify some set of gRNAs. Considering this and previous CRISPR-Cas activity analysis^{27,71}, we speculate that a computational model based on RNP or mRNA-gRNA complexes could outperform the predictive power of RNAtargeting for CRISPR-RfxCas13d activity in zebrafish embryos and enhance the precision when selecting highly active gRNAs in vivo. Beyond zebrafish embryos, this model could be additionally applied for other biotechnological or biomedical applications where these transient approaches could be used.

Fourth, we have analyzed the potential collateral activity of CRISPR-RfxCas13d in zebrafish embryos previously detected in vitro and in vivo^{30,32–36}. We have now characterized this effect in different molecular and physiological contexts by employing transient RNA-targeting approaches such as RNP complexes and RfxCas13d mRNA-

gRNA formulations during early zebrafish embryogenesis. Importantly, we confirmed that CRISPR-RfxCas13d is specific, and relevant collateral effects only occur when targeting extremely abundant ectopic RNAs such as *gfp* mRNA. We found that the toxicity and the physiological consequences of the collateral activity increased with the concentration of the *gfp* transcript as described in mammalian cells mRNA^{32,33} (i.e., 50 pg of *gfp* mRNA injected per embryo: 10,000 TPM at 6 hpf, Fig. 5E–G). Interestingly, even though the depletion of lower amounts of *gfp* mRNA (i.e., 10 pg per embryo) caused a deregulation of the transcriptome and 28S rRNA fragmentation, it did not induce a developmental defect. Indeed, targeting highly abundant endogenous mRNAs triggered an even fainter 28S rRNA fragmentation and did not generate an early embryogenesis alteration either (Fig. 5H, I, Supplementary Fig. 8C, D). These findings suggest that ectopic RNAs can elicit much more collateral and toxic effects in vivo than endogenous transcripts as reported in mammalian cell cultures^{32,35}. Nevertheless, when extremely abundant mRNAs are targeted by CRISPR-RfxCas13d RNP complexes in zebrafish embryos, a simple in vitro 28S rRNA cleavage assay can be used to detect even a weak collateral activity without developmental defects (Supplementary Fig. 8C, D). In addition, a subset of IVTted gRNAs can trigger toxicity in vivo that resembles collateral activity consequences observed when targeting extremely abundant and ectopic mRNA. However, this deleterious response is specifically due to the in vitro transcription reaction since the same gRNA when chemically synthesized did not generate any toxic effect while maintaining a similar efficiency of mRNA depletion (Fig. 2, Supplementary Fig. 3). Although a similar effect has been described in mammalian cells for IVTted gRNAs from CRISPR-SpCas9 and CRISPR-LbCas12a systems where 5′ triphosphate from IVTted gRNAs induced interferon response^{30,51} this was not the trigger of the developmental defects in zebrafish embryos. Why this subset of gRNAs for RfxCas13d induces toxicity during zebrafish embryogenesis depending on whether they are chemically synthesized or in vitro transcribed remains to be determined. A potential explanation could be that byproducts from the IVT reaction that generate these gRNAs⁷² could trigger this deleterious effect. Although, we demonstrated that chemically synthesized gRNAs do not induce developmental defects nor toxicity, they are more expensive than IVTted gRNAs and their use can be limited due to this higher cost. Therefore, in case of using IVTted gRNAs we have optimized a fast and straight-forward in vitro assay to determine their potential toxic activity that allows to screen for reliable gRNAs to be used in vivo. Notably, our results may suggest that the toxic effect triggered by IVTted gRNAs could be specifically associated to CRISPR-RfxCas13d system (Supplementary Fig. 12). However, the possibility that some IVTted gRNAs for DjCas13d or other CRISPR-Cas RNA-targeting systems could induce toxicity in vivo cannot be excluded and

this will be uncovered with the continued use of these technologies. Nevertheless, we have demonstrated that toxic IVTed gRNAs for RfxCas13d can be replaced by IVTed gRNAs for DjCas13d. Therefore, beyond our optimized protocol to detect toxic IVTed gRNAs for RfxCas13d, another possibility could be the use of IVTed gRNAs and CRISPR-DjCas13d system.

Indeed, and as an *in vivo* alternative to RfxCas13d specially when targeting extremely abundant transcripts, we have compared the activity of three RNA-targeting CRISPR-Cas systems that showed less or absent collateral activity when gRNAs and Cas were expressed from strong and constitutive promoters^{26,32,65}. While Hf-RfxCas13d³² exhibited low targeting activity (Fig. 6A–C, I, Supplementary Fig. 9B–D), Cas7-11⁶⁵ and DjCas13d²⁶ were more active, the latter showing an efficiency comparable to RfxCas13d (Fig. 6A–C, I). Interestingly, a recent report pointed out that Hf-RfxCas13d activity was inferior than initially described likely due to the lower level of expression of this endonuclease used in this report⁷³. Accordingly, this report revealed that the concentration of CRISPR-RfxCas13d reagents in mammalian cell culture is crucial to induce collateral activity⁷³. Strikingly, we recapitulated these results using a limited amount of CRISPR-RfxCas13d RNP or mRNA-gRNA complexes that show an absence of toxic effects *in vivo* when targeting endogenous mRNAs² (Fig. 5H, I, Supplementary Fig. 8). Nevertheless, DjCas13d and Cas7-11 reduced or eliminated, respectively, the developmental defects during zebrafish embryogenesis and the transcriptomic deregulation observed when RfxCas13d was used to eliminate ectopic and highly expressed RNAs (Fig. 6J–L, Supplementary Fig. 9E–L and Supplementary Fig. 11). However, DjCas13d did not totally lack collateral activity when targeting extremely abundant and ectopic mRNAs, inducing a delay during early zebrafish embryogenesis and a decrease in fluorescence levels from a co-injected *dsred* mRNA control reporter. Interestingly, DjCas13d did not trigger a detectable 28S rRNA cleavage in these conditions, suggesting that this uncontrolled effect may be more efficiently or specifically generated by RfxCas13d. An additional alternative to CRISPR-Cas13 is type III CRISPR-Cas system based on Csm complexes that have been recently employed to target RNA in human cells with minimal off-targets⁷⁴. Although similar approaches have been used in zebrafish embryos⁷⁵, the multicomponent factor of this CRISPR-Cas system with several proteins forming a functional complex challenges its use as RNP particle or mRNA-gRNA formulation *in vivo*. Another possibility to avoid collateral activity may be the application of catalytically dead versions of Cas13 fused to translational inhibitors to silence specific mRNA expression, rather than depleting the transcript^{76,77}. Instead, we have focused on the characterization, optimization and comparison of recently described high-fidelity CRISPR-Cas systems to eliminate RNA but in an *in vivo* context and using transient formulations that could be employed in potential RNA-editing therapies^{78–85}. Further, it has been described that RfxCas13d induces an immune response in humans⁸⁶ that could challenge the biomedical applications of this technology. Whether DjCas13d or Cas7-11 trigger lower immunological effects is something that remains to be determined. In summary, we demonstrate that CRISPR-RfxCas13d is a robust, specific and efficient system to target RNAs in zebrafish embryos but both CRISPR-Cas7-11 and CRISPR-DjCas13d RNP complexes could also be employed specially when targeting exceptionally abundant RNAs, being Cas7-11 less efficient than DjCas13d.

Altogether, our optimizations will not only contribute to broadening and enhancing the use of RNA-targeting CRISPR-Cas approaches in zebrafish but will also pave the way to optimize this technology *in vivo* for multiple biomedical and biotechnological applications.

Methods

Zebrafish maintenance and ethics statements

All experiments performed with zebrafish conform to national and European Community standards for the use of animals in experimentation and were approved by the Ethical committees from the Pablo de Olavide University, CSIC and the Andalusian Government.

Zebrafish wild-type strains AB/Tübingen (AB/Tu) or *Tupfel long fin* (TLF) were maintained and bred under standard conditions⁸⁷. Natural mating of wild-type AB/Tu/TLF zebrafish adults (from 6 to 18 months) was used to collect the embryos for subsequent experiments. Selection of mating pairs was random from a pool of 10 males and 10 females. Zebrafish embryos were staged in hpf as described by Kimmel et al.⁸⁸. Zebrafish experiments at Stowers Institute were done according to the IACUC approved guidelines. Zebrafish embryos for micro-injections came from random parents (AB, TF and TLF, 6–25 months old) mating from 4 independent strains of a colony of 500 fish. The embryos were pooled from random 24 males and 24 females for each set of experiments.

Guide RNA design and *in vitro* transcription and mRNA generation

To design gRNAs used in this study (Supplementary Data 2–4) target mRNA sequences were analyzed *in silico* using RNAfold software⁸⁹ (<http://rna.tbi.univie.ac.at/cgi-bin/RNAWebSuite/RNAfold.cgi>) to select protospacers of 23 (or 30) nucleotides with high accessibility (low base-pairing probability from minimum free energy predictions) within the ORF (except for miR-430 and u4atac snRNA that are non-coding RNAs) in regions where the probability of intramolecular interactions was reduced to ultimate facilitate the accessibility of RfxCas13d-gRNA complex. MiR-430 gRNAs were specifically designed to target regions within pri-miR-430 outside the mature miRNA or pre-miRNA sequence. All designed gRNAs were synthesized by Synthego (Synthego Corp., CA, USA). cm-gRNAs contain 2'-O-methyl analogs and 3'-phosphorothioate internucleotide linkage in the last three nucleotides of the binding site. Three gRNAs targeting the same mRNA were co-injected, otherwise it is specified in figure legends. RfxCas13d IVTed gRNAs were generated using a universal primer containing a T7 promoter as previously described^{10,11} but the concentration of primers was reduced by ten-fold in the fill-in PCR (5 µL of 10 µM universal primer and 5 µL of 10 µM of specific primers for a 50 µL fill-in PCR). After the fill-in PCR, QIAquick PCR Purification Kit (Qiagen #28104) was used for DNA purification, followed by the IVT using AmpliScribe-T7 Flash Transcription kit (Epicentre). Finally, gRNA concentration was measured using QUBIT 4 spectrophotometer (Thermo Fisher Scientific). gRNAs sequences from *si:dkay-93m18.4* gRNA1, 2 and 3 used were the same (same specific oligo), but two versions of the universal oligo were created: (1) one version with the T7 promoter sequence and 2) one where the T7 promoter sequence was switched to T3 promoter as follows: T3-RfxCas13d universal AATTAACCCTCACTAAAGGTACCCC-TACCAACTGGTCGGGGTTTGAAC (see Supplementary Data 5). PCR reactions were done with the same settings as previously described for T7 gRNAs. *In vitro* transcription was performed with MAXIscript T7/T3 kit (Invitrogen AM1326) following the manufacturer's protocols. All other steps were performed as previously described for T7 gRNAs.

Each gRNA from CRISPR-RfxCas13d system includes a set of optimizations that have been described to increase the efficiency of low active gRNAs^{11,23}: a stem-loop disruption and 23 nt long spacers, except gRNAs targeting *hmg1a* and *hspa8* that do not contain the stem-loop disruption yet they showed a high level of target depletion (95.2 and 83.5 % respectively). gRNAs with 30 nt long spacers contained the stem-loop disruption as well.

DjCas13d and Cas7-11 spacers were designed as described above using RNAfold software with minor modifications, i.e., length of binding sites for DjCas13d and Cas7-11 gRNAs are 30- and 31-nt, respectively. Scaffold or direct repeat for these CRISPR-Cas systems were described in Wei et al.²⁶ and Ozcan et al.⁶⁵, respectively. DjCas13d T7 *in vitro* transcription protocol was the same as described above for RfxCas13d.

Heitag (RfxCas13d-hei) version⁵⁸ of RfxCas13d was generated by PCR with Q5 High-Fidelity DNA polymerase (M0491, New England Biolabs) and primers hei-tag_13d_NcoI_fwd and hei-tag_13d_SacII_rev containing a cmc tag, an oNLS and NcoI site in forward primer and an

oNLS and SacII site in reverse primer, and cloned into pT3TS-MCS (Addgene plasmid #31830) backbone after digestion with restriction enzymes NcoI and SacII and ligation with T4 DNA ligase (M0202, New England Biolabs). Similarly, bpNLS (bipartite NLS, mRfxCas13d-bpNLS; Liang et al.⁵⁷), optimized 2C-NLS (SV40 and nucleoplasmin long-NLP NLS, mRfxCas13d-2C-NLS; Liu et al.⁵⁵) and cmcy-2C-NLS (cmcy, SV40 and nucleoplasmin long-NLP NLS, cmcy-mRfxCas13d-2C-NLS; Wu et al.⁵⁶) versions of *RfxCas13d* mRNA were created by PCR using primers NcoI_13d_bpNLS_fwd/13d_bpNLS_SacII_rev, NcoI_13d_fwd/13d_2C-NLS_SacII_rev and NcoI_13d_cmcy_fwd/13d_2C-NLS_SacII_rev to add bipartite NLS signals in N- and C-terminal ends, SV40 and nucleoplasmin long (NLP) NLS signals in C-terminal end, and cmcy tag in N-terminal end and SV40 and NLP NLS signals in C-terminal end, respectively. Each fragment was then cloned into pT3TS-NLS-RfxCas13d (Addgene plasmid #141321) backbone after digestion with restriction enzymes NcoI and SacII. All primers are listed in Supplementary Data 6. High-fidelity version of RfxCas13d (Hf-RfxCas13d) was generated by site-directed mutagenesis using QuikChange Multi Site-Directed Mutagenesis kit (Agilent), following manufacturer's instructions, and replicating the amino acid changes described in Tong et al.³² (N2V8 version). Primers are listed in Supplementary Data 6.

To generate *RfxCas13d*, *RfxCas13d-NLS*, *RfxCas13d-hei*, *RfxCas13d-bpNLS*, *RfxCas13d-2C-NLS*, *cmcy-RfxCas13d-2C-NLS*, and *Hf-RfxCas13d* mRNAs, the DNA templates were linearized using XbaI and mRNA was synthesized using the mMachine T3 kit (Ambion) for 2 h. IVTted mRNAs were then DNase-treated for 20 min with TURBO-DNase at 37 °C, purified using the RNeasy Mini Kit (Qiagen), and quantified using Nanodrop™ 2000 (Thermo Fisher Scientific).

gRNA CIP treatment

Sidkey-93m18.4 gRNAs in vitro transcribed with T7 polymerase were treated with quick-CIP (NEB #M0525S) based on Kim et al.⁵¹. For each 20 µg of gRNA, 500 U of quick-CIP and 200 U of RNase inhibitor were used. gRNAs were incubated at 37 °C for 3 h and then purified with the Monarch RNA cleanup kit (NEB #T2040S) or the Zymo RNA Clean and Concentrator 25 kit (Zymo R1017) following the standard cleanup protocol for total RNA with minimum elution volumes. *Brd4* gRNA IVTted with T7 polymerase was treated with quick-CIP (NEB #M0525S) and following the protocol described in Wienert B et al.⁵⁰. 20 U of CIP was added per 20 µL of sample volume and incubated for 3 h at 37 °C. Samples were then DNase-treated for 20 min with TURBO-DNase at 37 °C and purified using the RNeasy Mini Kit (Qiagen) following the manufacturer's instructions. After purification, CIP-treated gRNAs were injected into zebrafish embryos as previously described for T7 gRNAs.

Protein purification

The expression vector pET28b was used to clone genes for Hf-RfxCas13d, DjCas13d, and Cas7-11 proteins and were transformed into *E. coli* Rosetta DE3 pRare competent cells (70954, EMD Millipore). Hf-RfxCas13d ORF was cloned into pET28b vector after NcoI/NotI restriction enzyme digestion. DjCas13d ORF was codon optimized for zebrafish using iCodon⁹⁰ (www.iCodon.org), purchased from IDT, and cloned into pET28b vector after NcoI / NotI restriction enzyme digestion. Cas7-11 ORF was PCR amplified from pDF0229-DiCas7-11 (Addgene plasmid #172506) with Q5 High-Fidelity DNA polymerase (M0491, New England Biolabs; primers listed in Supplementary Data 6) and cloned into pET28b. A freshly transformed colony was picked and grown overnight at 37 °C in LB supplemented with kanamycin and chloramphenicol. This culture was diluted 100 times and grown at 37 °C until an OD₆₀₀ = 0.5 was reached. At this point, cultures for Hf-RfxCas13d and DjCas13d expression were induced with IPTG at a final concentration of 0.1 mM and incubated for 3 h at 37 °C. Culture for Cas7-11 expression was cooled for 30 min at 4 °C, induced with IPTG at 0.3 mM, and cultured overnight at 18 °C. Protein purification was

performed as described in Hernández-Huertas et al.¹¹, from cell pellets lysed by sonication followed by two consecutive chromatography steps (Ni-affinity chromatography followed by size exclusion chromatography).

Zebrafish embryo microinjection, phenotype quantification, and image acquisition

One-cell stage zebrafish embryos were injected with 1–2 nL containing 300–600 pg of Cas13(s) mRNA or 3 ng of purified Cas protein and 300–1000 pg of gRNA (see Figure Legends for details in each experiment). From 10 to 100 pg of ectopic *gfp* mRNA and 75 pg of ectopic *dsRed* mRNA were injected for collateral activity determination. Cas proteins and gRNAs were injected in two rounds to maximize the amount of protein and gRNA (at the indicated concentrations) per injection. Sequences of used gRNAs are indicated in Supplementary Data 2–4.

For the miR-430 rescue experiment, mature miR-430 duplexes (Supplementary Data 7) were purchased from IDT and resuspended in RNase-free water. Embryos were injected with 1 nL of 2.5 or 5 µM miR-430 duplex solution (equimolar mix of 3 duplexes miR-430a, miR-430b, and miR-430c), using single-use aliquots.

Nanog loss-of-function phenotypes were evaluated at 6 hpf: 30% epiboly, 50% epiboly, germ ring, and shield stages correspond to 4.6, 5.3, 5.7, and 6 hpf in non-injected embryos growing in standard conditions, respectively. *Tbxta-no-tail* or *noto* loss-of-function phenotypes were evaluated at 28 hpf. Class I: short tail (least extreme), Class II: absence of notochord and short tail (medium level), and Class III: absence of notochord and extremely short tail (most extreme). *Rx3*, loss-of-function phenotypes were evaluated at 48 hpf. Mild: smaller eye(s) (least extreme), Severe: absence of one eye (medium level), and No-eye: absence of both eyes (most extreme). *Tyrosinase*, *albino* (*slc45a2*), and *golden* (*slc24a5*) loss-of-function phenotypes (reduced or lack of pigmentation) were evaluated at 48 hpf: Mild (least extreme), Severe (medium level), and Albino-like (most extreme). *Smad5* loss-of-function phenotypes were evaluated at 24 hpf. *Tbx6* (*fss*) loss-of-function phenotypes were evaluated at 20 hpf differentiating between Mild (least extreme, only some fussed somites) and Severe (most extreme, most somites fussed). Representative pictures of described phenotypes are found in Fig. 1C and Supplementary Fig. 1A.

Zebrafish embryo phenotypes and fluorescent pictures were analyzed using an Olympus SZX16 stereoscope and photographed with a Nikon DS-F13 digital camera. Images were processed with NIS-Elements D 4.60.00 software. Phenotypes were quantified at 6, 24, or 48 hpf. GFP and DsRed fluorescence were quantified using Fiji (ImageJ) software, using 15 embryos separated in three different images (5 embryos per quantified image). Images were converted to 16-bit, background fluorescence was subtracted and fluorescence levels were referred to the ones from embryos injected only with reporter mRNAs.

Protein sample preparation and Western Blot

Twenty embryos were collected at 6 h post-injection and washed twice with deysolting buffer (55 mM NaCl, 1.8 mM KCl, and 1.25 mM NaHCO₃). Then, samples were incubated for 5 min with orbital shaking and centrifuged at 300 × g for 30 s. The supernatant was removed and embryos were washed with buffer (110 mM NaCl, 3.5 mM KCl, 10 mM Tris-HCl pH 7.4, and 2.7 mM CaCl₂). Finally, embryos were centrifuged again, and the supernatant was removed. The pellet was resuspended in SDS-PAGE sample buffer (160 mM Tris-HCl pH 8, 20% Glycerol, 2% SDS, 0.1% bromophenol blue, 200 mM DTT).

Sample separation by SDS-PAGE electrophoresis was performed using 10% TGX Stain-Free™ Fast Cast™ Acrylamide Solutions (Bio-Rad). After electrophoresis, protein gel was activated in a Chemidoc MP (Bio-Rad) and blotted onto a nitrocellulose membrane using the Trans-Blot Turbo Transfer System (Bio-Rad). The membrane was blocked for 1 h at room temperature in Blocking Solution (5% fat-free

milk in 50 mM Tris-Cl, pH 7.5, 150 mM NaCl (TBS) with 1% Tween 20). Primary antibody Anti-HA (I1867423001, Roche) and secondary antibody anti-mouse HRP-labeled (A5278, Sigma-Aldrich) were diluted 1:1000 and 1:5000 respectively in Blocking Solution. The membrane was incubated in primary antibody solution overnight at 4 °C. After primary antibody incubation, the membrane was washed three times in TBS with 1% Tween 20 (TTBS) for 10 min and incubated with the secondary antibody for 60 min at room temperature. Washes were performed as with primary antibody. The protein detection was done with Clarity™ Western ECL Substrate (Bio-Rad) and images were acquired using a ChemiDoc MP (Bio-Rad).

qRT-PCR

Ten zebrafish embryos per biological replicate were collected and snap-frozen in liquid nitrogen to analyze the expression level of the targeted mRNAs and pri-miR-430 by qRT-PCRs at the described hpf in figures or figure legends. Total RNA was isolated using the RNeasy ZOL™ Reagent protocol as described in the manufacturer's instructions (Qiagen Biotech). The cDNA was synthesized from 1000 ng of total RNA using iScript cDNA synthesis kit (Bio-Rad), following the manufacturer's protocol. cDNA was 1/5 diluted and 2 µL was used per sample in a 10 µL reaction containing 1.5 µL of forward and reverse primers (2 mM each; Supplementary Data 7), 5 µL of SYBR® Premix Ex Taq (Tli RNase H Plus) (Takara) and run in a CFX connect instrument (Bio-Rad). PCR cycling profile consisted of a denaturing step at 95 °C for 30 s and 40 cycles at 95 °C for 10 s and 60 °C for 30 s. *taf15* or *efl1a* mRNAs stably expressed along early development were used as normalization controls for $2^{-\Delta\Delta C_t}$ analysis. To quantify *si:dkey-93m18.4* mRNA levels from Fig. 2 and Supplementary Fig. 3, 15 embryos per replicate were collected and snap-frozen in tubes containing 350 µL of TRIzol. Total RNA isolation was performed with the Zymo Direct-zol Microprep kit according to the manufacturer's recommendations (including the DNase digestion step), eluting in 20 µL of nuclease-free H₂O. Superscript IV was used for reverse transcription of ~1 µg of total RNA, and the resulting cDNA was diluted 1:20 for RT-qPCR. RT-qPCR was run in technical triplicate on a 384-well plate setup by a Tecan robot and run on a QuantStudio 7 workstation using PerfeCTa® SYBR® Green FastMix® (Quantabio). *cdk2ap2* mRNA stably expressed along early development was used as a normalization control for $2^{-\Delta\Delta C_t}$ analysis. Gene-specific oligos for *si:dkey-93m18.4* and *cdk2ap2* are listed in Supplementary Data 7.

To analyze the relative levels of each mature miR-430 and *u4atac* snRNA, 15 embryos per replicate were snap-frozen, and total RNA samples and RNA samples enriched in small RNAs were obtained with mirVana mRNA Isolation Kit (AM1561, ThermoFisher Scientific) following the manufacturer's protocol. For total RNA samples, cDNA was synthesized as described above. For RNA samples enriched in small RNA, cDNA was synthesized from 100 ng of RNA using iScript Select cDNA synthesis kit (Bio-Rad), following the manufacturer's protocol and using the following miRNA universal primer (5'-GCAGGTC-CAGTTTTTTTTTTTTTCTACCCC-3'), 2 µL of cDNA were used per sample in a 10 µL reaction containing 1.5 µL of forward and reverse primers (2 mM each; Supplementary Data 7), 5 µL of SYBR® Premix Ex Taq (Tli RNase H Plus) (Takara) and run in a CFX connect instrument (Bio-Rad). PCR cycling profile consisted of a denaturing step at 95 °C for 30 s and 40 cycles at 95 °C for 10 s and 60 °C for 30 s. miR-430b mRNA was used as normalization control for $2^{-\Delta\Delta C_t}$ analysis for *u4atac* KD experiment and *u4atac* snRNA for mature miR-430 KD.

In vivo RNA integrity analysis

RNA samples containing 10 embryos and purified using standard TRIzol protocol, were submitted to RNA integrity analysis using Bioanalyzer Agilent 2100 (Supplementary Fig. 3B, Supplementary Fig. 7A, B, G, Supplementary Fig. 8C, G, Supplementary Fig. 9K, L and Supplementary Fig. 12G).

For in vivo RNA integrity analysis of IVTed gRNAs (Fig. 2C–E, H, Supplementary Figs. 8D and 12C, F), 300–500 ng of total RNA was heat denatured for 2 min at 70 °C, placed on ice, and then loaded onto an RNA Nano Chip for the Agilent Bioanalyzer 2100, prepared according to manufacturer's protocol. Electrophoresis results were exported as image representations and as raw.csv files of fluorescence intensity and time, including the ladder. Using R-Studio, the ladder was fit with a second-degree polynomial and the polynomial fit was used to calculate the size of the species in each experimental lane, resulting in a table with of traces of all RNA species represented by size in nucleotides and fluorescence intensity. Size values fit with regions of the second-degree polynomial with a negative derivative (including those of the 25 nt lower marker) were then trimmed from these traces. A custom pipeline based around findpeaks (pracma library) to detect, identify, quantify, and analyze up to the three most prominent RNA species (18S, 28S, long 28S cleavage product) in each trace (based on max-normalization) was developed and employed. If a species was absent based on our peak calling results, the intensity within the search window for that species was averaged and this mean intensity was used in calculating the “28S rRNA integrity ratio”. In order to obtain reliable results of 28S rRNA integrity ratio, all the samples must be run in the same gel electrophoresis within the 2100 Bioanalyzer.

In vitro RNA integrity analysis

A single in vitro experimental rRNA integrity assay (Supplementary Fig. 3C, D) consists of the following components in a 10 µL reaction: 60 ng of RfxCas13d protein, 500 ng of gRNA of interest, 300–500 ng zebrafish total RNA, 1 µL of 10X CutSmart Buffer (New England Biolabs), and nuclease-free water to 10 µL. Reactions were incubated at 28.5 °C for 45 min, heat denatured for 2 min at 70 °C, placed on ice, and then 1 µL of the reaction was loaded onto an RNA Nano Chip for the Agilent Bioanalyzer 2100, prepared according to the manufacturer's protocol. Electrophoresis results were exported as image representations and as raw.csv files of fluorescence intensity and time, including the ladder.

Using R-Studio, the ladder was fit with a second-degree polynomial and trimmed traces as above. These traces were further timed to remove the gRNA peak. In vivo, rRNA analysis pipeline (see above) was modified and based around findpeaks (pracma library) to detect, identify, quantify, and analyze up to the 3 most prominent RNA species (18S, 28S, long 28S cleavage product) in each in vitro trace (based on max-normalization). Due to the 10x lower input of RNA in the in vitro traces, a short 28S cleavage product was not detected above the baseline. If a species was absent based on our peak calling results, the intensity within the search window for that species was averaged and this mean intensity was used in calculating the “28S rRNA integrity ratio”. In order to obtain reliable results of 28S rRNA integrity ratio, all the samples must be run in the same gel electrophoresis within the 2100 Bioanalyzer.

RNAseq libraries and analysis

Between 10 to 20 zebrafish embryos per biological replicate were collected at 4 or 6 hpf and snap-frozen. For analyzing pri-miR-430 targets stability with optimized NLS version of RfxCas13d (Fig. 3) and to determine the collateral activity induced by different CRISPR-Cas RNA targeting systems (Figs. 5 and 6, Supplementary Fig. 11), total RNA was isolated using standard TRIzol protocol as described in the manufacturer's instructions (ThermoFisher Scientific) and quantified using the Qubit fluorometric quantification (#Q10210, ThermoFisher Scientific).

For pri-miR-430 targets stability, 200 ng (except for 13.5 ng and 174 ng, for two samples) of high-quality total RNA was used, as assessed using the Bioanalyzer (Agilent), with the NEBNext Poly(A) mRNA Magnetic Isolation Module (NEB, Cat. No. E7490L) at a 1/3rd reaction volume. Purified mRNA was processed using the NEBNext Ultra II

Directional RNA Library Prep Kit for Illumina (NEB, Cat. No. E7760L) at a 1/10th reaction volume. Poly(A) isolated mRNA was resuspended in 2.25 μ L fragmentation mix and fragmented for 15 min at 94 °C then placed on ice for 2 min. First-strand cDNA synthesis was performed by manually transferring 1 μ L of the fragmented mRNA into a 384-well Armadillo PCR microplate (ThermoFisher, AB2396), containing 1 μ L of the First-Strand cDNA synthesis reaction master mix aliquoted by the Mosquito HV Genomics (SPT Labtech) nanoliter liquid-handling instrument. Second-strand synthesis was completed per protocol at the miniaturization scale and the cDNA was purified using the SPRIselect bead-based reagent (Beckman Coulter, Cat. No. B23318) at 1.8X with the Mosquito HV and eluted in 5 μ L of 0.1X TE. Libraries were generated using the NEBNext Ultra II Directional RNA Library Prep Kit at a 1/10th reaction volume⁹¹ starting with 5 μ L of cDNA. Adapters were ligated by adding 500 nL of NEBNext Universal Adaptor diluted at 20-fold in the supplied adapter dilution buffer. The adapter-ligated material was PCR amplified with 14 cycles using the NEBNext Multiplex Oligos for Illumina (96 Unique Dual Index Primer Pairs) (NEB, Cat. No. E6442S) and the indexed libraries were purified using SPRIselect at 0.9X with the Mosquito HV and eluted in 10 μ L of 0.1X TE.

For collateral activity RNAseq, mRNAseq libraries were generated from 100 ng (or \leq 100 ng; RfxCas13d and DjCas13d) or 200 ng (or 40 ng for one sample; Cas7-11) of high-quality total RNA and analyzed using the Bioanalyzer (Agilent). Libraries were made according to the manufacturer's directions using a 25-fold (or 100-fold) dilution of the universal adapter and 12–16 cycles of PCR per the respective masses with the NEBNext Ultra II Directional RNA Library Prep Kit for Illumina (NEB, Cat. No. E7760L), the NEBNext Poly(A) mRNA Magnetic Isolation Module (NEB, Cat. No. E7490L), and the NEBNext Multiplex Oligos for Illumina (96 Unique Dual Index Primer Pairs) (NEB, Cat. No. E6440S) and purified using the SPRIselect bead-based reagent (Beckman Coulter, Cat. No. B23318).

For RNAseq analysis of IVTed gRNAs and their counterparts targeting *si:dkay-9m18.4* with CRISPR-RfxCas13d (Fig. 2 and Supplementary Fig. 3), mRNA was captured manually from 100 ng of high-quality total RNA, as assessed using the Fragment Analyzer (Agilent Technologies), with the Watchmaker mRNA Library Prep Kit (Watchmaker Genomics, Cat. No. 7BK0001-096) at a 1/5th reaction volume. Poly(A) isolated mRNA was resuspended in a 5.4 μ L fragmentation mix. mRNA was fragmented for 10 min at 85 °C, according to the manufacturer's directions then placed on a 384 magnetic block (SPT Labtech, Cat. No. 3268-02008) to separate the fragmented mRNA. First-strand cDNA synthesis was performed by manually transferring 5 μ L of the fragmented mRNA into a 384-well PCR microplate (Eppendorf, Cat. No. 951020702), containing 2 μ L of the first-strand cDNA synthesis reaction master mix. Second-strand synthesis was carried out per protocol at the miniaturization scale. Truncated stubby adapters were ligated by adding 1 μ L of IDT xGen Stubby Adapter diluted to 1 μ M in Buffer EB (QIAGEN, Cat. No. 19086). The adapter-ligated material was purified using the SPRIselect bead-based reagent (Beckman Coulter, Cat. No. B23318) at 0.7X with the Mosquito HV Genomics (SPT Labtech) nanoliter liquid-handling instrument and eluted in 4 μ L of Buffer EB. The purified adapter-ligated libraries were PCR amplified with 13 cycles using the IDT xGen Unique Dual Indexing primers (IDT, Cat. No. 10005921) and the indexed libraries were purified using SPRIselect at 1X with the Mosquito HV and eluted in 10 μ L of Buffer EB.

Generated short fragment libraries for Figs. 2, 3, 5 and 6 and Supplementary Figs. 3 and 11 were checked for quality and quantity using the Bioanalyzer and the Qubit Flex Fluorometer (Life Technologies). Equal molar libraries from Figs. 3 and 5 and Supplementary Fig. 11 were pooled, quantified, and converted to process on the Singular Genomics G4 with the SG Library Compatibility Kit, following the “Adapting Libraries for the G4—Retaining Original Indices” protocol. The converted pool was sequenced on an F3 flow cell (Cat. No. 700125) on the G4 instrument with the PP1 and PP2 custom index primers

included in the SG Library Compatibility Kit (Cat. No. 700141), using Instrument Control Software 23.08.1-1 with the following read length: 8 bp Index1, 100 bp Read1, and 8 bp Index2. Following sequencing, sgdemux 1.2.0 was run to demultiplex reads for all libraries and generate FASTQ files. Equal molar libraries from Fig. 2 and Supplementary Fig. 3 were pooled, quantified, and sequenced on the AVITI (Element Biosciences) on a 2 \times 75 Cloudbreak Freestyle High-Output flow cell (Cat. No. 860-00004), using AVITI OS 2.3.0 with the following read length: 8 bp Index1, 8 bp Index2, 76 bp Read1, and 76 bp Read2. Following sequencing, Bases2Fastq was run to demultiplex reads for all libraries and generate FASTQ files.

To determine the number of gRNAs that can be injected together to detect highly efficient gRNAs with CRISPR-RfxCas13d (Supplementary Fig. 5) and then to analyze the prediction of ex vivo computational models using in vivo data from 200 gRNAs injected in sets of 25 gRNAs (Fig. 4 and Supplementary Fig. 6), total RNA was isolated at 4 hpf using Direct-zol RNA Miniprep Kit (#R2050, Zymo Research) following manufacturer's instructions and quantified using the Qubit fluorometric quantification (#Q10210, ThermoFisher Scientific). cDNA was generated from 1.25 ng (2.5 ng for two replicates of RfxCas13d control samples) of high-quality total RNA, as assessed using the Bioanalyzer (Agilent), according to manufacturer's directions for the SMART-seq v4 Ultra Low Input RNA Kit (Takara, 634891) at a 1/8th reaction volume (1/4th reaction volume for two replicates of RfxCas13d control) and using the Mantis (Formulatrix) nanoliter liquid-handling instrument to pipette the reagents for cDNA synthesis. Libraries were generated manually (or with the Mosquito HV Genomics (SPT Labtech) nanoliter liquid-handling instrument for RNAseq in Fig. 4 and Supplementary Fig. 6), using the Nextera XT DNA Library Preparation Kit (Illumina, FC-131-1096) at 1/8th reaction volumes (or 1/4th reaction volume for two replicates of RfxCas13d control) paired with IDT for Illumina DNA/RNA UD Indexes Set A (Illumina, 20027213), and purified using the Ampure XP bead-based reagent (Beckman Coulter, Cat. No. A63882). The resulting short fragment libraries were checked for quality and quantity using the Bioanalyzer and Qubit Fluorometer (ThermoFisher). Equal molar libraries were pooled, quantified, and sequenced on a High-Output flow cell of an Illumina NextSeq 500 instrument using NextSeq Control Software 2.2.0.4 (or NextSeq Control Software 4.0.1 for RNAseq in Fig. 4 and Supplementary Fig. 6) with the following read length: 70 bp Read1, 10 bp i7 Index and 10 bp i5 Index. Following sequencing, Illumina Primary Analysis version NextSeq RTA 2.4.11 (or version NextSeq RTA 2.11.3.0 for RNAseq in Fig. 4 and Supplementary Fig. 6) and Secondary Analysis version bcl2fastq2 v2.20 were run to demultiplex reads for all libraries and generate FASTQ files.

RNAseq reads were demultiplexed into Fastq format allowing up to one mismatch using Illumina bcl-convert 3.10.5. Reads were aligned using STAR version 2.7.3a to *Danio rerio* reference genome *danRer11* from the University of California at Santa Cruz (UCSC) with GFP exogenous sequence incorporated in its index using Ensembl 106 gene models.

TPM (Transcript per Million) values were generated using RSEM version 1.3.0. Fold change for each gene was calculated using deseq2 (1.42.0) R package after filtering genes with a count of less than 10 reads in all control libraries. The resulting *p*-values were adjusted with the Benjamini–Hochberg method using the R function *p.adjust*. For collateral activity assay, genes with less than 20 counts in the control conditions were filtered.

Gene set enrichment analysis

Differential expression analysis from RNAseq data was ranked based on fold change compared to control conditions and used as input for gene set enrichment analysis (GSEA)^{92,93}, resulting in a Normalized Enrichment Score with its adjusted *p*-value. Orthologous genes from the Human Gene Set HALLMARK_INTERFERON_GAMMA_RESPONSE⁹⁴ were selected to analyze the interferon response upon *si:dkay-93m18.4*

mRNA KD. GSEA analyses were conducted using the R package clusterProfiler (v. 4.10.0).

Guide RNAs efficacy estimation

To determine the number of gRNAs that could be injected together in zebrafish embryos to detect highly active gRNAs, we co-injected 10 and 25 gRNAs together with RfxCas13d protein in one-cell stage zebrafish embryos (Supplementary Data 3). Then, RNAseq at 4 hpf was performed as described earlier and gRNAs were divided into quintiles according to their activity (q5 and q1 being the most and the least efficient gRNAs, respectively, Supplementary Fig. 5).

To calculate gRNAs efficacy in vivo, 200 gRNAs (Supplementary Data 4) were injected in eight different sets of 25 gRNAs together with RfxCas13d protein in one-cell stage zebrafish embryos. Two to three gRNAs targeting the same mRNA (75 mRNAs in total) were designed as described above, specifically to the longest transcript isoform. gRNAs from set 1, set 2, and set 3 targeted the same 25 mRNAs, gRNAs from set 4, set 5, and set 6 targeted the following 25 mRNAs, and gRNAs from set 7 and set 8 targeted the last 25 mRNAs. For instance, *aebp2* transcript, one of the first 25 mRNAs, was targeted with gRNA1 (13d_aebp2_1) in set 1, gRNA2 (13d_aebp2_1) in set 2 and gRNA3 (13d_aebp2_1) in set 3. Then, in vivo, gRNA efficacy for each individual gRNA was calculated as the inverse of the Fold Change, obtained from RNAseq from zebrafish embryos at 4 hpf.

The most recent and updated computational models to predict CRISPR-RfxCas13d activity generated from ex vivo cell culture data, TIGER²⁴, DeepCas13²⁵, and RNAtargeting²⁶, were used to estimate gRNA efficacy. Since RNAtargeting generates gRNA spacer sequences of 30 nt length, the first 23 nt from the 5' end were used to make them comparable to our gRNAs and to other models. Out of 200 gRNA used in this experiment, including three gRNAs as negative controls, 191 were compatible to be analyzed in all computational models. Then, the performance of each prediction model was evaluated using Pearson's correlation coefficient. Ex vivo cell culture data from 396 gRNAs targeting *gfp* mRNA²³ was used as an external control.

Statistics and reproducibility

All statistical analyses were performed without predetermining sample size. The experiments were not randomized, and investigators were not blinded to allocation during experiments and outcome assessment. No data was excluded from the analysis. Number of embryos, replicates and experiments are indicated in figures and/or figure legends.

For phenotypes derived from embryo microinjections, Xi-square or Fisher statistical analyses were undertaken using GraphPad Prism 8 (La Jolla, CA, USA). For qRT-PCR, GFP and DsRed fluorescence levels, Grubbs's test was performed first for outlier's identification and then, One-way ANOVA or T-test statistical analyses were performed. *p* values are indicated in figures or figure legends. Non-parametric Mann–Whitney *U* statistical test was performed to compare high (top 5) and low (bottom 5) active gRNAs scores (Fig. 4C–E).

p values and distances (*D*, maximal vertical distance between the compared distribution) for the comparison of the cumulative distribution of RNA levels at 6 hpf (Fig. 3C) were calculated using Kolmogorov–Smirnov Tests by dgof (v 1.4) in R package.

All information regarding the specific number or biological replicates, independent experiments, and type of statistical analysis performed in each figure or supplementary figure is listed in Supplementary Data 1.

Reporting summary

Further information on research design is available in the Nature Portfolio Reporting Summary linked to this article.

Data availability

Sequencing data have been uploaded to Gene Expression Omnibus (GEO) (Series [GSE270724](https://doi.org/10.1038/s41467-025-57792-9)). All other data are available in the main text or the supplementary information. Source data is provided with this paper. Key plasmids have been deposited in Addgene. Source data are provided with this paper.

Code availability

The codes generated in this study to perform 28S rRNA ratio and correlations for gRNA activity prediction have been deposited in the GitHub database [https://github.com/ajtreich/danrer_28SrRNA_integrity.git] and [<https://github.com/morenomateoslab/RfxCas13d.git>], respectively. Code is available for use under the open-source GNU GENERAL PUBLIC LICENSE and MIT license respectively.

References

- Konermann, S. et al. Transcriptome engineering with RNA-targeting type VI-D CRISPR effectors. *Cell* **173**, 665–676.e14 (2018).
- Wessels, H. H. et al. Efficient combinatorial targeting of RNA transcripts in single cells with Cas13 RNA Perturb-seq. *Nat. Methods* **20**, 86–94 (2023).
- Montero, J. J. et al. Genome-scale pan-cancer interrogation of lncRNA dependencies using CasRx. *Nat. Methods* **21**, 584–596 (2024).
- Tieu, V. et al. A versatile CRISPR-Cas13d platform for multiplexed transcriptomic regulation and metabolic engineering in primary human T cells. *Cell* **187**, 1278–1295.e20 (2024).
- Ding, Y., Tous, C., Choi, J., Chen, J. & Wong, W. W. Orthogonal inducible control of Cas13 circuits enables programmable RNA regulation in mammalian cells. *Nat. Commun.* **15**, 1572 (2024).
- Zhou, H. et al. Glia-to-neuron conversion by CRISPR-CasRx alleviates symptoms of neurological disease in mice. *Cell* **181**, 590–603.e16 (2020).
- Powell, J. E. et al. Targeted gene silencing in the nervous system with CRISPR-Cas13. *Sci. Adv.* **8**, 2485 (2022).
- Yu, L. et al. Systemic evaluation of various CRISPR/Cas13 orthologs for knockdown of targeted transcripts in plants. *Genome Biol.* **25**, 307 (2024).
- Huang, F. et al. Integrative analysis identifies the atypical repressor E2F8 as a targetable transcriptional activator driving lethal prostate cancer. *Oncogene* **44**, 481–493 (2025).
- Kushawah, G. et al. CRISPR-Cas13d induces efficient mRNA knockdown in animal embryos. *Dev. Cell* **54**, 805–817.e7 (2020).
- Hernandez-Huertas, L. et al. Optimized CRISPR-RfxCas13d system for RNA targeting in zebrafish embryos. *STAR Protoc.* **3**, 101058 (2022).
- Hernandez-Huertas, L. et al. CRISPR-RfxCas13d screening uncovers Bckdk as a post-translational regulator of the maternal-to-zygotic transition in teleosts. *bioRxiv*, <https://doi.org/10.1101/2024.05.22.595167> (2024).
- Pescador, G. et al. Protein profiling of zebrafish embryos unmasks regulatory layers during early embryogenesis. *Cell Rep.* **43**, 114769 (2024).
- Kushawah, G. et al. Critical role of spatio-temporally regulated maternal RNAs in zebrafish embryogenesis. *bioRxiv* <https://doi.org/10.1101/2024.11.07.622483> (2024).
- Zhu, W. et al. Reading and writing of mRNA m6A modification orchestrate maternal-to-zygotic transition in mice. *Genome Biol.* **24**, 67 (2023).
- Shangguan, H., Huang, X., Lin, J. & Chen, R. Knockdown of Kmt2d leads to growth impairment by activating the Akt/β-catenin signaling pathway. *G3 Genes Genomes Genet.* **14**, jkad298 (2024).
- Cheng, R. et al. Modification of alternative splicing in bovine somatic cell nuclear transfer embryos using engineered CRISPR-Cas13d. *Sci. China Life Sci.* **65**, 2257–2268 (2022).

18. Bi, D. et al. CRISPR/Cas13d-mediated efficient KDM5B mRNA knockdown in porcine somatic cells and parthenogenetic embryos. *Reproduction* **162**, 149 (2021).
19. Del Prado, J. A.-N. et al. Comparing robotic and manual injection methods in zebrafish embryos for high-throughput RNA silencing using CRISPR-RfxCas13d. *Biotechniques* **76**, 183–191 (2024).
20. Nishimura, T., Takahashi, E. & Fujimoto, T. Sterilization of fish through adaptable gRNAs targeting *dnd1* using CRISPR-Cas13d system. *Aquaculture* **593**, 741269 (2024).
21. Treichel, A. J. & Bazzini, A. A. Casting CRISPR-Cas13d to fish for microprotein functions in animal development. *iScience* **25**, 105547 (2022).
22. Huang, Y. et al. CRISPR-dCas13-tracing reveals transcriptional memory and limited mRNA export in developing zebrafish embryos. *Genome Biol.* **24**, 15 (2023).
23. Wessels, H. H. et al. Massively parallel Cas13 screens reveal principles for guide RNA design. *Nat. Biotechnol.* **38**, 722–727 (2020).
24. Wessels, H. H. et al. Prediction of on-target and off-target activity of CRISPR-Cas13d guide RNAs using deep learning. *Nat. Biotechnol.* **42**, 628–637 (2024).
25. Cheng, X. et al. Modeling CRISPR-Cas13d on-target and off-target effects using machine learning approaches. *Nat. Commun.* **14**, 1–14 (2023).
26. Wei, J. et al. Deep learning and CRISPR-Cas13d ortholog discovery for optimized RNA targeting. *Cell Syst.* **14**, 1087–1102.e13 (2023).
27. Moreno-Mateos, M. A. et al. CRISPRscan: designing highly efficient sgRNAs for CRISPR-Cas9 targeting in vivo. *Nat. Methods* **12**, 982–988 (2015).
28. Doench, J. G. et al. Optimized sgRNA design to maximize activity and minimize off-target effects of CRISPR-Cas9. *Nat. Biotechnol.* **34**, 184–191 (2016).
29. Kim, H. K. et al. Deep learning improves prediction of CRISPR-Cpf1 guide RNA activity. *Nat. Biotechnol.* **36**, 239–241 (2018).
30. Buchman, A. et al. Programmable RNA targeting using CasRx in flies. *CRISPR J.* **3**, 164 (2020).
31. Huynh, N., Depner, N., Larson, R. & King-Jones, K. A versatile toolkit for CRISPR-Cas13-based RNA manipulation in *Drosophila*. *Genome Biol.* **21**, 279 (2020).
32. Tong, H. et al. High-fidelity Cas13 variants for targeted RNA degradation with minimal collateral effects. *Nat. Biotechnol.* **41**, 108–119 (2023).
33. Shi, P. et al. Collateral activity of the CRISPR/RfxCas13d system in human cells. *Commun. Biol.* **6**, 334 (2023).
34. Ai, Y., Liang, D. & Wilusz, J. E. CRISPR/Cas13 effectors have differing extents of off-target effects that limit their utility in eukaryotic cells. *Nucleic Acids Res.* **50**, E65 (2022).
35. Kelley, C. P., Haerle, M. C. & Wang, E. T. Negative autoregulation mitigates collateral RNase activity of repeat-targeting CRISPR-Cas13d in mammalian cells. *Cell Rep.* **40**, 111226 (2022).
36. Li, Y. et al. The collateral activity of RfxCas13d can induce lethality in a RfxCas13d knock-in mouse model. *Genome Biol.* **24**, 20 (2023).
37. Meeske, A. J., Nakandakari-Higa, S. & Marraffini, L. A. Cas13-induced cellular dormancy prevents the rise of CRISPR-resistant bacteriophage. *Nature* **570**, 241–245 (2019).
38. East-Seletsky, A. et al. Two distinct RNase activities of CRISPR-C2c2 enable guide-RNA processing and RNA detection. *Nature* **538**, 270–273 (2016).
39. Abudayyeh, O. O. et al. C2c2 is a single-component programmable RNA-guided RNA-targeting CRISPR effector. *Science* **353**, aaf5573 (2016).
40. Zhang, C. et al. Structural basis for the RNA-guided ribonuclease activity of CRISPR-Cas13d. *Cell* **175**, 212 (2018).
41. Slaymaker, I. M. et al. High-resolution structure of Cas13b and biochemical characterization of RNA targeting and cleavage. *Cell Rep.* **26**, 3741 (2019).
42. Escot, S. et al. Nance-Horan-syndrome-like 1b controls mesodermal cell migration by regulating protrusion and actin dynamics during zebrafish gastrulation. *Commun. Biol.* **8**, 328 (2025).
43. Méndez-Mancilla, A. et al. Chemically modified guide RNAs enhance CRISPR-Cas13 knockdown in human cells. *Cell Chem. Biol.* **29**, 321–327.e4 (2021).
44. White, R. J. et al. A high-resolution mRNA expression time course of embryonic development in zebrafish. *eLife* **6**, e30860 (2017).
45. Lee, M. T. et al. Nanog, Pou5f1 and SoxB1 activate zygotic gene expression during the maternal-to-zygotic transition. *Nature* **503**, 360–364 (2013).
46. Lele, Z., Bakkers, J. & Hammerschmidt, M. Morpholino phenocopies of the swirl, snailhouse, somitabun, minifin, silberblick, and pipetail mutations. *Genesis* **30**, 190–194 (2001).
47. Schulte-Merker, S. et al. Expression of zebrafish goosecoid and no tail gene products in wild-type and mutant no tail embryos. *Development* **120**, 843–852 (1994).
48. Loosli, F. et al. Loss of eyes in zebrafish caused by mutation of *chokh/rx3*. *EMBO Rep.* **4**, 894 (2003).
49. Nikaido, M. et al. Tbx24, encoding a T-box protein, is mutated in the zebrafish somite-segmentation mutant fused somites. *Nat. Genet.* **31**, 195–199 (2002).
50. Wienert, B., Shin, J., Zelin, E., Pestal, K. & Corn, J. E. In vitro-transcribed guide RNAs trigger an innate immune response via the RIG-I pathway. *PLoS Biol.* **16**, e2005840 (2018).
51. Kim, S. et al. CRISPR RNAs trigger innate immune responses in human cells. *Genome Res.* **28**, 367–373 (2018).
52. Sun, Q., Hao, Q. & Prasanth, K. V. Nuclear long noncoding RNAs: key regulators of gene expression. *Trends Genet.* **34**, 142 (2018).
53. Guh, C. Y., Hsieh, Y. H. & Chu, H. P. Functions and properties of nuclear lncRNAs-from systematically mapping the interactomes of lncRNAs. *J. Biomed. Sci.* **27**, 1–14 (2020).
54. Pillay, S., Takahashi, H., Carninci, P. & Kanhere, A. Antisense RNAs during early vertebrate development are divided in groups with distinct features. *Genome Res.* **31**, 995–1010 (2021).
55. Liu, P. et al. Enhanced Cas12a editing in mammalian cells and zebrafish. *Nucleic Acids Res.* **47**, 4169–4180 (2019).
56. Wu, Y. et al. Highly efficient therapeutic gene editing of human hematopoietic stem cells. *Nat. Med.* **25**, 776 (2019).
57. Liang, F. et al. SpG and SpRY variants expand the CRISPR toolbox for genome editing in zebrafish. *Nat. Commun.* **13**, 1–10 (2022).
58. Thumberger, T. et al. Boosting targeted genome editing using the hei-tag. *eLife* **11**, e70558 (2022).
59. Giraldez, A. J. et al. Zebrafish MiR-430 Promotes Deadenylation And Clearance Of Maternal MRNAs. *Science* **312**, 75–79 (2006).
60. Giraldez, A. J. et al. MicroRNAs regulate brain morphogenesis in zebrafish. *Science* **308**, 833–838 (2005).
61. Hadzhiev, Y. et al. The miR-430 locus with extreme promoter density forms a transcription body during the minor wave of zygotic genome activation. *Dev. Cell* **58**, 155–170.e8 (2023).
62. Medina-Muñoz, S. G. et al. Crosstalk between codon optimality and cis-regulatory elements dictates mRNA stability. *Genome Biol.* **22**, 1–23 (2021).
63. Vejnar, C. E. et al. Genome wide analysis of 3' UTR sequence elements and proteins regulating mRNA stability during maternal-to-zygotic transition in zebrafish. *Genome Res.* **29**, 1100–1114 (2019).
64. Khatri, D. et al. Deficiency of the minor spliceosome component U4atac snRNA secondarily results in ciliary defects in human and zebrafish. *Proc. Natl. Acad. Sci. USA* **120**, e2102569120 (2023).
65. Özcan, A. et al. Programmable RNA targeting with the single-protein CRISPR effector Cas7-11. *Nature* **597**, 720–725 (2021).
66. Rossi, A. et al. Genetic compensation induced by deleterious mutations but not gene knockdowns. *Nature* **524**, 230–233 (2015).

67. Housden, B. E. et al. Loss-of-function genetic tools for animal models: cross-species and cross-platform differences. *Nat. Rev. Genet.* **18**, 24–40 (2016).
68. Bosch, B. et al. Genome-wide gene expression tuning reveals diverse vulnerabilities of *M. tuberculosis*. *Cell* **184**, 4579–4592.e24 (2021).
69. Saunders, L. M. et al. Embryo-scale reverse genetics at single-cell resolution. *Nature* **623**, 782 (2023).
70. Shen, W. et al. Comprehensive maturity of nuclear pore complexes regulates zygotic genome activation. *Cell* **185**, 4954–4970.e20 (2022).
71. Haeussler, M. et al. Evaluation of off-target and on-target scoring algorithms and integration into the guide RNA selection tool CRISPOR. *Genome Biol.* **17**, 148 (2016).
72. Triana-Alonso, F. J., Dabrowski, M., Wadzack, J. & Nierhaus, K. H. Self-coded 3'-extension of run-off transcripts produces aberrant products during in vitro transcription with T7 RNA polymerase. *J. Biol. Chem.* **270**, 6298–6307 (1995).
73. Hart, S. K. et al. Precise RNA targeting with CRISPR–Cas13d. *Nat. Biotechnol.* <https://doi.org/10.1038/s41587-025-02558-3> (2025).
74. Colognori, D., Trinidad, M. & Doudna, J. A. Precise transcript targeting by CRISPR–Csm complexes. *Nat. Biotechnol.* **41**, 1256 (2023).
75. Fricke, T. et al. Targeted RNA knockdown by a type III CRISPR–Cas complex in zebrafish. *CRISPR J.* **3**, 299 (2020).
76. Li, S. et al. Screening for functional circular RNAs using the CRISPR–Cas13 system. *Nat. Methods* **18**, 51–59 (2021).
77. Apostolopoulos, A. et al. dCas13-mediated translational repression for accurate gene silencing in mammalian cells. *Nat. Commun.* **15**, 2205 (2024).
78. Zhu, Y., Zhu, L., Wang, X. & Jin, H. RNA-based therapeutics: an overview and prospectus. *Cell Death Dis.* **13**, 1–15 (2022).
79. Balwani, M. et al. Phase 3 trial of RNAi therapeutic givosiran for acute intermittent porphyria. *N. Engl. J. Med.* **382**, 2289–2301 (2020).
80. Schultheis, B. et al. First-in-human phase I study of the liposomal RNA interference therapeutic Atu027 in patients with advanced solid tumors. *J. Clin. Oncol.* **32**, 4141–4148 (2014).
81. Kumar, S. et al. RNA-targeting strategies as a platform for ocular gene therapy. *Prog. Retin. Eye Res.* **92**, 101110 (2023).
82. Li, J. et al. Cas13b-mediated RNA targeted therapy alleviates genetic dilated cardiomyopathy in mice. *Cell Biosci.* **14**, 4 (2024).
83. Keng, C. T. et al. AAV–CRISPR–Cas13 eliminates human enterovirus and prevents death of infected mice. *EBioMedicine* **93**, 104682 (2023).
84. Li, J. et al. A high-fidelity RNA-targeting Cas13 restores paternal Ube3a expression and improves motor functions in Angelman syndrome mice. *Mol. Ther.* **31**, 2286–2295 (2023).
85. Cui, Z. et al. Cas13d knockdown of lung protease Ctsl prevents and treats SARS-CoV-2 infection. *Nat. Chem. Biol.* **18**, 1056–1064 (2022).
86. Tang, X. Z. E., Tan, S. X., Hoon, S. & Yeo, G. W. Pre-existing adaptive immunity to the RNA-editing enzyme Cas13d in humans. *Nat. Med.* **28**, 1372 (2022).
87. Daude, N. et al. Knockout of the prion protein (PrP)-like Sprn gene does not produce embryonic lethality in combination with PrPC-deficiency. *Proc. Natl. Acad. Sci. USA* **109**, 9035–9040 (2012).
88. Kimmel, C. B., Ballard, W. W., Kimmel, S. R., Ullmann, B. & Schilling, T. F. Stages of embryonic development of the zebrafish. *Dev. Dyn.* **203**, 253–310 (1995).
89. Lorenz, R. et al. ViennaRNA Package 2.0. *Algorithms Mol. Biol.* **6**, 26 (2011).
90. Diez, M. et al. iCodon customizes gene expression based on the codon composition. *Sci. Rep.* **12**, 1–16 (2022).
91. Mildrum, S. et al. High-throughput minitaturized RNA-seq library preparation. *J. Biomol. Tech.* **31**, 151–156 (2020).
92. Mootha, V. K. et al. PGC-1 α -responsive genes involved in oxidative phosphorylation are coordinately downregulated in human diabetes. *Nat. Genet.* **34**, 267–273 (2003).
93. Subramanian, A. et al. Gene set enrichment analysis: a knowledge-based approach for interpreting genome-wide expression profiles. *Proc. Natl. Acad. Sci. USA* **102**, 15545–15550 (2005).
94. Liberzon, A. et al. The Molecular Signatures Database (MSigDB) hallmark gene set collection. *Cell Syst.* **1**, 417–425 (2015).

Acknowledgements

We thank all members of the Moreno-Mateos laboratory for their intellectual and technical support. This work was supported by Ramon y Cajal (RyC-2017-23041), PID2021-127535NB-I00, CNS2022-135564 and CEX2020-001088-M grants funded by MICIU/AEI/ 10.13039/501100011033 by “ERDF A way of making Europe” (“ERDF/EU”), and by ESF Investing in your future from Ministerio de Ciencia, Innovación y Universidades and European Union (M.A.M.-M.). This work has also been co-financed by the Spanish Ministry of Science and Innovation with funds from the European Union NextGenerationEU (PRTR-C17.I1) and the Regional Ministry of University, Research, and Innovation of the Autonomous Community of Andalusia within the framework of the Biotechnology Plan applied to Health. The Moreno-Mateos lab was also funded by the European Regional Development Fund (FEDER 80% of the total funding) by the Ministry of Economy, Knowledge, Business and University, of the Government of Andalusia, within the framework of the FEDER Andalusia 2014-2020 operational program within the objective “Promotion and generation of frontier knowledge and knowledge oriented to the challenges of society, development of emerging technologies (grant UPO-1380590)” and by the Fondo Europeo de Desarrollo Regional (FEDER) and Consejería de Transformación Económica, Industria, Conocimiento y Universidades de la Junta de Andalucía, within the operative program FEDER Andalucía 2014-2020 (01—Refuerzo de la investigación, el desarrollo tecnológico y la innovación, grant P20_00866). M.A.M.-M. was the recipient of the Genome Engineer Innovation 2019 Grant from Synthego. The CABD is an institution funded by University Pablo de Olavide, Consejo Superior de Investigaciones Científicas (CSIC), and Junta de Andalucía. I.M-S. was a recipient of the Margarita Salas Postdoctoral contract funded by “NextGenerationEU”, Plan de Recuperación, Transformación y Resiliencia and Ministerio de Ciencia, Innovación y Universidades (recualificación del sistema universitario español 2021-2023, Pablo de Olavide University Call). L.H.-H. and D.N.-C. were recipients of Ayudas para contratos predoctorales para la formación de doctores (Ministerio de Ciencia e Innovación) funded by MICIU/AEI/ 10.13039/501100011033 and FSE invierte en tu futuro and FSE. C.G.-M. was funded with Ayudas captación, incorporación y movilidad de capital humano de I+D+i, Junta de Andalucía (POSTDOC 21_00667). P.M.M.G. was funded by a postdoctoral fellowship from Junta de Andalucía (DOC_00397). This study was supported by the Stowers Institute for Medical Research. A.A.B. was awarded a US National Institutes of Health grant (NIH-R01 GM136849 and NIH R21OD034161). A.J.T. was supported by the US National Institute of Health: F31HD110268. This work was completed as part of thesis research for A.J.T. and G.d.S.P., Graduate School of the Stowers Institute for Medical Research. This work was supported by grant PID2021-125682NB-I00 to M.A.N. funded by MICIU/AEI/ 10.13039/501100011033 and by FEDER, UE; funds were also provided by Instituto de Salud Carlos III (CIBERER, CB19/07/00038 to M.A.N.) and Generalitat Valenciana (Prometeo 2021/45). M.A.N. also acknowledges financial support from the Spanish State Research Agency, through the “Severo Ochoa Program” for Centres of Excellence in R&D Grant CEX2021-001165-S funded by MCIN/AEI/ 10.13039/501100011033. M.J.M. was supported by grant PID2020-120463RB-I00 funded by the Spanish Ministerio de Ciencia e Innovación. We thank our colleague Francisco J. Guerra (Stowers Institute and CABD) for the initial research on Cas7-11, Amanda Lawlor and Kate Hall (Stowers Institute) for their technical work on RNA sequencing, and Cielo Centola for the help with illustrations (CABD).

Author contributions

M.A.M.-M. conceived the project and designed the research. I.M.-S., L.H.-H., and D.N.-C. performed most of the experiments. C.G.-M., A.C.-R., and M.J.M. contributed to the CRISPR-Cas7-11 and CRISPR-DjCas13d experiments and analysis. A.J.T., G.d.S.P., and G.K. performed part of the experiments and analyzed the results from in vitro-transcribed gRNAs assays in zebrafish. L.T.-G. and A.D.-M. performed protein purifications. J.A.W.II produced the synthetic gRNAs. R.E. and A.P. contributed to RNA libraries generation and sequencing. K.H. helped with cm-gRNAs section together with J.G. and M.A.N. who also contributed to the optimization of RfxCas13d-NLS. P.M.-G. performed gRNA activity prediction analysis and computational models' comparison. M.A.M.-M., I.M.-S., L.H.-H., and D.N.-C. carried out data analysis with the help of A.A.B. M.A.M.-M. and I.M.-S. wrote the manuscript with the contribution of L.H.-H., D.N.-C., and A.A.B. and with the input from the other authors. All authors reviewed and approved the manuscript.

Competing interests

K.H. and J.A.W.II were both employees and shareholders in Synthego Corporation at the time of this work. The rest of authors declare no competing interests.

Additional information

Supplementary information The online version contains supplementary material available at <https://doi.org/10.1038/s41467-025-57792-9>.

Correspondence and requests for materials should be addressed to Miguel A. Moreno-Mateos.

Peer review information *Nature Communications* thanks Carolyn Shembrey and the other, anonymous, reviewer(s) for their contribution to the peer review of this work. A peer review file is available.

Reprints and permissions information is available at <http://www.nature.com/reprints>

Publisher's note Springer Nature remains neutral with regard to jurisdictional claims in published maps and institutional affiliations.

Open Access This article is licensed under a Creative Commons Attribution-NonCommercial-NoDerivatives 4.0 International License, which permits any non-commercial use, sharing, distribution and reproduction in any medium or format, as long as you give appropriate credit to the original author(s) and the source, provide a link to the Creative Commons licence, and indicate if you modified the licensed material. You do not have permission under this licence to share adapted material derived from this article or parts of it. The images or other third party material in this article are included in the article's Creative Commons licence, unless indicated otherwise in a credit line to the material. If material is not included in the article's Creative Commons licence and your intended use is not permitted by statutory regulation or exceeds the permitted use, you will need to obtain permission directly from the copyright holder. To view a copy of this licence, visit <http://creativecommons.org/licenses/by-nc-nd/4.0/>.

© The Author(s) 2025